Food Research International 212 (2025) 116397

Contents lists available at ScienceDirect

Food Research International

journal homepage: www.elsevier.com/locate/foodres

Therapeutic potential of (1 → 4)-linked glucuronoglucan from an edible brown mussel *Perna indica*: A promising candidate for anti-inflammatory and antidyslipidemic nutraceuticals

Ashwin Ashok Pai [a,b], Kajal Chakraborty [a,1,*], Archana Raj [c], Bibu John Kariyil [c,*], Shubhajit Dhara [a,b], Anoopraj R. [d]

[a] *Marine Biotechnology, Fish Nutrition and Health Division, ICAR-Central Marine Fisheries Research Institute, Ernakulam North, P.B. No. 1603, Cochin 682018, Kerala State, India*

[b] *Department of Chemistry, Mangalore University, Mangalagangothri 574199, Karnataka State, India*

[c] *Department of Veterinary Pharmacology & Toxicology, College of Veterinary and Animal Sciences, Kerala Veterinary and Animal Sciences University, Mannuthy 680651, Thrissur, Kerala State, India*

[d] *Department of Veterinary Pathology, College of Veterinary and Animal Sciences, Kerala Veterinary and Animal Sciences University, Mannuthy 680651, Thrissur, Kerala State, India*

ARTICLE INFO

Keywords:
Edible brown mussel *Perna indica*
(1 → 4)-linked glucuronoglucan
Chronic ailments
Functional foods

ABSTRACT

The brown mussel, *Perna indica* (Kuriakose & Nair, 1976), family *Mytilidae*, is harvested along the southwest coast of India for its rich nutritional composition and therapeutic potential. This study highlights the role of PIP-1, a (1 → 4)-linked glucuronoglucan derived from *Perna indica* composed of repeating pyranose units of *β*-D-glucose (Glc*p*) and *α*-D-glucuronic acid (GlcA*p*), in alleviating chronic diseases. PIP-1 demonstrated potent anti-inflammatory activity by attenuating 5-lipoxygenase (5-LOX) and cyclooxygenases (COXs) ($IC_{50} \leq 1.5$ mg/mL), with preferential COX-2 selectivity and reduced nitric oxide levels (IC_{50} 2.9 μg/mL) in lipopolysaccharide-induced macrophages. *In vivo* models demonstrated that PIP-1, at higher dose, significantly reduced acute paw edema (91 % within 5 h) induced by carrageenan and chronic paw edema (77 % within day 10) induced by formalin. PIP-1 exhibited a potent antihypercholesterolemic effect by inhibiting 3-hydroxy-3-methylglutaryl-CoA reductase (IC_{50} 0.86 mg/mL) and significantly reduced triglyceride levels by 8–54 % in Caco-2 cells. *In vivo* studies showed that PIP-1 reduced total cholesterol by 68 % and triglycerides by 25 % in dyslipidemic rats after 48 h of acute study. In chronic studies, reductions of 19 % in total cholesterol and 46 % in triglycerides were observed after 45 days. The therapeutic potential of PIP-1 largely stems from its electronegative groups, which increase its total polar surface area, thereby facilitating receptor interactions through Van der Waals forces and modulating key metabolic pathways. Given its notable anti-inflammatory and antidyslipidemic effects, PIP-1 presents a promising source for developing nutraceutical products designed to alleviate chronic ailments.

1. Introduction

The rich biodiversity and ecosystem services of marine environments drive sustainable development, emphasizing the urgent need for conservation to secure future food security and economic stability (Farmery et al., 2022). *Perna indica* (Kuriakose & Nair, 1976), commonly known as the brown mussel, are native to the tropical and subtropical regions of the Atlantic Ocean, Western Indian Ocean, and Mediterranean Sea. This species naturally inhabits rocky shores, mangroves, and estuaries, where it provides essential ecosystem services that support diverse organisms (Gardner et al., 2016; Silva Dos Santos et al., 2022). Brown mussel serves as an important food source for coastal communities and is extensively farmed in countries like India, Philippines, Thailand, China, Venezuela, and New Zealand (Gardner et al., 2016). Rich in eicosapentaenoic acid (EPA), docosahexaenoic acid (DHA), protein, and minerals, they serve as excellent therapeutic agents, promoting good health and aiding in the deterrence and cure of various human diseases (Dalin et al., 2021; Jeyasanta et al., 2018). Furthermore, the carbohydrate profile of

* Corresponding authors.
E-mail addresses: kajal_cmfri@yahoo.com, kajal.chakraborty@icar.gov.in (K. Chakraborty), bibujohn@kvasu.ac.in (B.J. Kariyil).
[1] Primary Corresponding Author

https://doi.org/10.1016/j.foodres.2025.116397
Received 7 December 2024; Received in revised form 22 March 2025; Accepted 15 April 2025
Available online 17 April 2025

P. indica is notably high during its mature stage compared to other *Perna* species. As filter feeders that primarily consume phytoplankton, *P. indica* also functions as an effective environmental pollution indicator (Jeyasanta et al., 2018). Beyond its nutritional value, *P. indica* possesses significant pharmacological potential, and its organic extract has demonstrated efficacy against pathogens, such as *Staphylococcus* and *Escherichia* species (Jeyasanta et al., 2020). Mariculture experiments have validated the potential for large-scale farming, achieving production rates of 150 t per hectare and an average yield of 12 kg per meter of rope (Appukuttan & Nair, 1983). The establishment of standardized culture methods, such as rope and raft farming, has enhanced the consistency of *P. indica* aquaculture, ensuring a stable supply of raw materials (Appukuttan et al., 1989).

Chronic diseases are slow-progressing, long-term, non-infectious disorders that arise from various factors, including physiological, genetic, behavioural, and environmental influences. Chronic inflammation, dyslipidemia, and diabetes are closely linked to many diseases, serving as key contributing factors in their development (Budreviciute et al., 2020). Recently, the rising cost of health foods essential for managing dyslipidemia and inflammatory diseases has led individuals to consume low-quality, high-fat, and triglyceride-rich foods that lack bioactive omega-3 fatty acids, fiber, and polyphenols, thereby exacerbating chronic inflammation and dyslipidemia (Shehzad et al., 2011). Additionally, a sedentary lifestyle, smoking, and excessive alcohol consumption induce oxidative stress, further promoting inflammation and lipid imbalances. Increasing exposure to pollutants and toxins also contributes to oxidative stress, compounding the risk of metabolic disturbances that lead to the development of cardiovascular diseases (CVDs), obesity, metabolic syndrome, and type 2 diabetes (Seyedsadjadi & Grant, 2020; Shehzad et al., 2011). Inflammation is a crucial immune defense mechanism that involves the migration of immune cells, such as macrophages and neutrophils, to sites of tissue impairment, where they release chemokines and cytokines. However, when the immune system fails to neutralize harmful triggers or adequately resolve the inflammatory response, inflammation can become chronic (Nigam et al., 2023). Autoimmune or abnormal immune responses can trigger conditions, such as obesity, diabetes, rheumatoid arthritis, inflammatory bowel diseases, non-alcoholic fatty liver disease (NAFLD), multiple organ dysfunction syndrome, and neurodegenerative disorders (Budreviciute et al., 2020; Martins, 2017). Conventional treatment for chronic inflammation includes non-steroidal anti-inflammatory drugs (NSAIDs), corticosteroids, and inhibitors of inflammatory mediators, such as histamine and serotonin. However, chronic use of these agents can lead to gastrointestinal toxicity, nephrotoxicity, and hepatotoxicity (Ali et al., 2023). Similarly, dyslipidemia is a chronic condition marked by increased levels of pro-atherogenic indices, such as total cholesterol (TC), very low-density lipoprotein (VLDL), low-density lipoprotein (LDL), triglycerides (TG), and phospholipids, alongside decreased levels of the anti-atherogenic index and high-density lipoprotein (HDL) (Jing et al., 2022). Current therapeutic strategies for dyslipidemia primarily include statins, fibrates, and cholesterol absorption inhibitors, which work by reducing lipid levels through mechanisms, such as the inhibition of HMG-CoA reductase (HMGCR), blocking cholesterol absorption in the intestine, and modulating lipid metabolism. However, these medications are often associated with adverse effects, including hepatotoxicity and myopathy, limiting their long-term use and patient adherence (Dybiec et al., 2023). Autoimmune responses can disrupt lipid metabolism, leading to increased triglyceride levels and the oxidation of LDL into oxidized LDL (oxLDL), which contributes to atherogenesis. Additionally, autoimmune effects on pancreatic β-cells result in their destruction, leading to type 1 diabetes mellitus (T1DM), where the inherent ability to produce insulin is impaired (Tirado & Yassin, 2017). Although T1DM accounts for only about 10 % of diabetes cases worldwide, its incidence is increasing and it often manifests early in life (Paschou et al., 2018). The World Health Organization (WHO) recommends utilizing at least two servings of seafood each week to promote a healthy lifestyle and reduce the risk of chronic ailments, as studies have shown a link between increased seafood intake and lower disease rates (Jamioł-Milc et al., 2021).

In the past few years, nutraceuticals, especially those derived from marine sources, have been developed as health foods for managing non-communicable diseases with minimal side effects. Marine-derived nutraceuticals, such as Cadalmin™ Green Mussel Extract (GMe), Oyster Plus, Lyprinol®, and Aquatone are rich in bioactive polysaccharides, omega-3 fatty acids, peptides, and antioxidants. These products are marketed for managing inflammation and dyslipidemia, thereby enhancing immunity, alleviating joint pain, and promoting overall cardiovascular health (Chakraborty & Joy, 2020). Polysaccharides, a class of secondary metabolites, exhibit a wide range of therapeutic applications, largely influenced by their structural diversity. Their bioactivity is determined by factors, such as monosaccharide composition, functional groups, glycosidic linkages, molecular weight, degree of branching, and chain conformation (Wang et al., 2022). Mussels produce polysaccharides with hypolipidemic, immunomodulatory, anticancer, antioxidant, and anticoagulant activities, attributed to their unique structures, including glucan analogs, glycosaminoglycans, and sulfated glycosaminoglycans (Chen et al., 2019; Tan et al., 2023). The presence of electronegative groups and (1 → 3)/(1 → 4) linkages in polysaccharides may enhance their recognition and binding to cell membrane receptors on macrophages, including complement receptor 3 (CR3), dendritic cell-associated C-type lectin-1 (Dectin), and Toll-like receptors (TLR2 and TLR4). This interaction can modulate the inflammatory cascade initiated by macrophage signaling pathways (Huang et al., 2019; Suchecka et al., 2017). Beyond their high bioactivity, polysaccharides are generally non-toxic, biodegradable, and highly bioavailable, making them excellent therapeutic agents (Benalaya et al., 2024).

In light of the aforementioned aspects, this study aims to isolate a polysaccharide, PIP-1, from the seafood brown mussel *P. indica*. The PIP-1 was characterized through advanced spectroscopic methods, and its bioactivity was linked to physicochemical properties using ADME (absorption, distribution, metabolism, and excretion) molecular modeling software. A preliminary therapeutic assessment of PIP-1 was carried out by evaluating its capacity to inhibit free radicals. Furthermore, the inhibition capacity of PIP-1 against cyclooxygenases (COX), 5-lipoxygenase (5-LOX), HMGCR, angiotensin-converting enzyme, α-amylase, and α-glycosidase was investigated. The *in vitro* anti-inflammatory potential of PIP-1 was evaluated by measuring nitric oxide (NO) secretion in lipopolysaccharide (LPS)-induced macrophage cells, while its anti-dyslipidemic effects were assessed by monitoring triglyceride levels in dyslipidemic Caco-2 cells. The acute and chronic anti-inflammatory efficacy of PIP-1 was assessed by monitoring paw edema induced by carrageenan and formalin in Swiss albino mice. Similarly, hypoglycemic potential was measured by monitoring blood glucose levels under normal conditions in Sprague Dawley (SD) rats and acute and chronic hypoglycemic effect was studied in streptozotocin (STZ)-induced SD rats. The *in vivo* acute and chronic antidyslipidemic potential was investigated by examining the effects of PIP-1 on elevated triglyceride and cholesterol levels induced by tyloxapol and high-fat high-cholesterol (HFHC) diet in SD rats.

2. Materials and methods

2.1. Reagents and instrumentation

Reagents, such as trichloroacetic acid (TCA; CAS: 76–03-9), diethylaminoethyl (DEAE) cellulose 52 (CAS: 9013-34-7), α-amylase (CAS: 9000-90-2), and α-glucosidase (CAS: 9001-42-7) were obtained from Sisco Research Laboratories Pvt. Ltd. (Mumbai, India). Cyclooxygenase-1 (COX-1; C0733), cyclooxygenase-2 (COX-2; C0858), anhydrous dimethyl sulfoxide (DMSO; 276,855), pyridine (270970), diclofenac sodium salt (PHR1144), acarbose (PHR1253), and zileuton (PHR2555)

were sourced from Sigma Aldrich (St. Louis, MO, USA). Trifluoroacetic acid (TFA; CAS: 76–05-1) and HPLC-grade solvents were acquired from Spectrochem Pvt. Ltd. (Mumbai, India). Minimum Essential Medium (MEM; AL182A), carrageenan (GRM1576), indomethacin (TC465), ascorbic acid (PCT0207), streptozotocin (TC418), tyloxapol (RM3009), and 0.25 % trypsin (TCL165) were procured from HiMedia Laboratories (LLC, Kelton, PA, USA). Fetal bovine serum (FBS; A5670801) was purchased from Thermo Fisher Scientific (Waltham, MA, USA). Details regarding equipments are provided elsewhere (Supplementary material S1).

2.2. Collection of P. indica

10 kg of *P. indica* were collected from the Vizhinjam Sea Coast, Thiruvananthapuram (8.3932° N, 77.0046° E) in Kerala, South India, during the February–March period of 2024. The brown mussels were thoroughly washed, deshelled, macerated, and lyophilized to obtain brown mussel powder, which was then stored at −20 °C.

2.3. Extraction of crude polysaccharide from brown mussel

Brown mussel powder was subjected to aqueous extraction twice at 80–90 °C for 4 h with continuous mechanical stirring. The resulting water extract was clarified by centrifugation (ST 16 R, Thermo Fisher Scientific, Waltham, MA, USA), and the amount was then concentrated to one-tenth using rotary vacuum evaporation (Heidolph Hei-VAP Precision motor lift, Heidolph, Germany). The extract was treated with 5 % TCA and stored at 4 °C for 12 h to ensure complete deproteination. The precipitate formed was removed by centrifugation, and ice-cold ethanol, at four times the supernatant volume, was added to precipitate the crude polysaccharide (PIP). The mixture was then refrigerated at 4 °C overnight to facilitate the precipitation of polysaccharide. The resulting polysaccharide was freeze-dried (Martin Christ beta 2–8 LSC basic, Martin Christ, Germany) to obtain the PIP (Huang et al., 2021).

2.4. Fractionation and structural characterization of PIP

PIP underwent anion exchange fractionation using a DEAE-cellulose stationary phase in an open glass column (250 mm × 40 mm). Initially, 40 g of DEAE-cellulose was hydrated in 300 mL of water for 4 h, packed into the chromatographic column, and washed with double-distilled water. A solution containing 4 g of PIP dissolved in 15 mL of double-distilled water was eluted using a gradient sodium chloride solution (0–0.4 M NaCl) (Gu et al., 2020). Total carbohydrate, sulfate, and uronic acid content of eluted fractions (PIP-1 to PIP-4) were analyzed (Supplementary material S2), and the corresponding profile was plotted (Fig. S1). The fraction with the highest carbohydrate content (PIP-1) was subjected to acid hydrolysis using 2 M TFA at 100 °C for 6 h. Fraction was freeze-dried and monosaccharide composition was analyzed using HPLC system (Shimadzu, Japan) (Supplementary material S3) (Bi et al., 2024). Glycosidic bond analysis was conducted on partially methylated alditol acetates (PMAAs) derived from the hydrolysate fraction through a series of steps, including methylation, hydrolysis, reduction, and acetylation (Supplementary material S4). GCMS (Shimadzu, Japan) was used to establish resultant PMAAs using the fragmentation patterns.

2.5. In vitro bioactivity assessment

The antioxidant activities of PIP and PIP-1 were assessed by measuring its inhibitory effects on 2,2-diphenyl-1-picrylhydrazyl (DPPH), 2,2′-azino-bis (3-ethylbenzothiazoline-6-sulfonic acid) (ABTS), and hydrogen peroxide (H_2O_2) radicals, as well as through an iron (Fe^{2+}) chelating assay. Anti-inflammatory activity was evaluated by calculating inhibition capacity against COX-1, 2 and 5-LOX enzymes. Anti-dyslipidemic potential was measured using HMGCR estimation kit, and antidiabetic efficacy was quantified by measuring inhibition capacity against α-amylase and α-glycosidase enzymes (detailed procedure is provided in the Supplementary material S5). The enzymatic inhibition activity was expressed as IC_{50} values, which are calculated using the following formula:

$$\text{Inhibition capacity } (\%) = \frac{A_C - A_S}{A_C} \times 100$$

This value denotes the concentration at which PIP, PIP-1, and standards inhibit the bioactivity of enzymes and radicals by 50 %. Ac represents the absorbance of the negative control, and A_S represents the absorbance of the test sample.

2.6. Cell culture

Murine macrophage RAW 264.7 cells and Caco-2 cells utilized in this study were procured from the National Centre for Cell Science (NCCS) in Pune, India. The cultivation and upkeep of these cells adhered to the detailed protocols provided in the Supplementary material S6.

2.7. Inhibition of NO levels by PIP-1 on LPS-induced macrophage cells

A stock solution of PIP-1 (5000 ppm) was prepared in anhydrous DMSO and subsequently diluted with Dulbecco's Modified Eagle Medium (DMEM) to obtain assay concentrations ranging from 1 to 10 μg/mL. These concentrations were selected from a broader range (0.01–160 μg/mL) based on their optimal bioactivity without cytotoxicity. Macrophage cells were plated into a 96-well plate at a density of 5000 cells per well. Subsequently, the culture medium was exchanged for a serum-free medium, and the cells were exposed to PIP-1 at the specified concentrations for 2 h. After the pre-treatment, the cells were treated with 1 μg/mL of LPS before being incubated for 24 h. The culture supernatants were then subjected to the Griess reaction to evaluate nitrite ion (NO_2^-) production. Indomethacin (10 μM) was used as standard. Further details regarding the nitrite assay can be found in the Supplementary material S7.

2.8. Variation in triglyceride levels in PIP-1 administered dyslipidemic Caco-2 cells

A stock solution of PIP-1 (5000 ppm) was prepared (5000 ppm) in anhydrous DMSO and then diluted with MEM to obtain assay concentrations ranging from 0.1 to 160 μg/mL, ensuring that the final concentration of DMSO in each well was maintained at 0.1 %. These concentrations were selected from a broader range (0.01–160 μg/mL) based on their optimal bioactivity without cytotoxicity. Caco-2 cells were plated into a 96-well plate at a density of 10,000 cells per well. The cells were incubated for 4 days with media change on alternate days. On the fourth day, aliquots of PIP-1 were added to the culture media, and cells were treated with varying concentrations of PIP-1. Triglyceride levels were then measured using a quantification kit (Agappe Diagnostics Ltd). Detailed protocols provided in the Supplementary material S8.

2.9. Experimental animals for in vivo studies

Swiss albino mice of both sexes, weighing between 25 and 30 g were procured from the Small Animal Breeding Station at the College of Veterinary and Animal Sciences (CVAS) in Thrissur, Kerala. Additionally, SD rats of either sex, weighing between 150 and 200 g, were procured from the Sree Chitra Tirunal Institute for Medical Sciences and Technology, Biomedical Wing, Trivandrum, Kerala. After a 7-day acclimatization period, the animals were given unrestricted access to standard pellet feed (SANFT, CVAS, Thrissur, Kerala) and provided with *ad libitum* filtered water. The animals were housed in polypropylene cages filled with corn cob bedding material and kept under a 12-h light-dark cycle at an ambient temperature of 19–25 °C and 45 % relative

humidity. The study followed rules and regulations specified by the Govt. of India's Committee for Control and Supervision of Experiments on Animals, India (CCSEA). The study protocol received the approval from the Institutional Animal Ethical Committee of the College of Veterinary and Animal Sciences, Mannuthy, Thrissur, Kerala, under sanction order numbers CVAS/MTY/IAEC/23/36 dated 15/3/2023, CVAS/MTY/IAEC/23/37 dated 15/3/2023, and CVAS/MTY/IAEC/23/51 dt. 13/09/2023.

2.10. Acute oral toxicity study

The acute toxicity assessment of PIP-1 was executed as per the guidelines outlined in the Organization for Economic Co-operation and Development (OECD) No. 420, specifically the Acute Oral Toxicity: Fixed Dose Procedure (Organization for Economic Co-operation and Development, 2002). After an overnight fast, PIP-1 was dissolved in corn oil and administered orally at an initial dose of 300 mg/kg body weight, with the animal observed for 24 h. Subsequently, the remaining animals received a dose of 2000 mg/kg b. wt., given sequentially with a 24 h interval between doses. The animals were carefully monitored throughout the study for any signs of mortality and clinical symptoms. Observations were monitored at specific intervals: within the first 10 min, then at 30 min, 1, 2, and 4 hours post-administration. This was followed by twice-daily mortality checks and daily assessments of clinical signs over a period of 14 days.

2.11. Acute and chronic anti-inflammatory activity assessment of PIP-1 administered Swiss albino mice using carageenan and formalin-induced paw edema model

The acute anti-inflammatory activity of PIP-1 was assessed by monitoring variation in paw edema in carrageenan-induced mice over a 5 h study period, while the chronic anti-inflammatory activity was assessed using a formalin-induced paw edema model over a 10-day study period. Two sets of 24 mice were categorized into 4 groups, each comprising 6 mice. (i) Carrageenan/formalin treatment group (sham group), (ii) indomethacin (10 mg/kg b. wt.) treated group, (iii) low dose (22 mg/kg b. wt.) PIP-1 treated group, and (iv) high dose (110 mg/kg b. wt.) PIP-1 treated group (Ou et al., 2019).

In the carrageenan-induced model, the percentage inhibition of paw thickness was monitored at 30 min, 1, 2, 3, 4, and 5 h, while in the formalin-induced model, paw thickness was measured daily from day 1 to day 10 for the treatment groups. After analysis, the animals from all the groups were sacrificed, and the paw edema feet from all the animals were dismembered and preserved in 10 % neutral buffered formalin for histopathological analysis. The detailed assessment procedure is provided in the Supplementary material S9.

2.12. Acute and chronic antidyslipidemia activity assessment of PIP-1 administered hyperlipidemic SD rats

The antidyslipidemic potential of PIP-1 was assessed in SD rats by measuring triglyceride and cholesterol levels in acute and chronic conditions. Acute dyslipidemia was studied using tyloxapol-induced rats and chronic dyslipidemia was studied using HFHC-diet-induced rats. For the study, two sets of 30 rats were distributed into 5 groups, each consisting of 6 rats. The groups belong to the (i) normal control group, (ii) hyperlipidemic control (sham) group, (iii) standard treated group, (iv) low dose (18 mg/kg b. wt.) PIP-1 administered group, and (v) high dose (90 mg/kg b. wt.) PIP-1 administered group (Rasouli et al., 2016). For the acute study, blood was collected at 0, 18, 24, 40, and 48 h, and for the chronic study blood was collected at 0^{th}, 15^{th}, 30^{th}, and 45^{th} day. Rats were humanely sacrificed and histopathology parameters of the liver, such as steatosis, lobular inflammation, and ballooning degeneration were analyzed. Kidney sections were examined for varying degrees of fatty change and vacuolar degeneration, while the parameters, such as fatty change, vacuolar degeneration, and myocardial necrosis were evaluated in the heart (Abdallah et al., 2015; Paget & Barnes, 1964).

2.13. Variation in blood glucose levels in normal SD rats

18 rats were categorized into 3 groups, each consisting of 6 rats. These three groups are: (a) normal control, (b) metformin administered, and (c) PIP-1 treatment group. After acclimatization, the rats were fasted overnight and evaluated the level of fasting glucose using a blood glucose monitoring system (El Hilaly & Lyoussi, 2002).

2.14. Acute and chronic antidiabetic activity assessment of PIP-1 in STZ-induced rats

The antidiabetic potential of PIP-1 was evaluated in SD rats by measuring blood glucose levels under both acute and chronic conditions in STZ-induced diabetic rats. Acute anti-diabetic activity was assessed by administering PIP-1 at doses of 54 and 270 mg/kg b. wt. during a 5 h study period. Chronic antidiabetic effects were evaluated by administering PIP-1 at doses of 18 and 90 mg/kg b. wt. over a 21-day study period. Two sets of 30 rats were divided into 5 groups, each consisting of 6 rats: (a) normal control, (b) hyperglycemic control (sham), (c) metformin-treated, (d) low-dose PIP-1, and (e) high-dose PIP-1. Blood samples were collected from the tail vein, and blood glucose levels were measured at 0–5 h for the acute study, and on days 0, 7, 14, and 21 for the chronic study using a blood glucose monitoring system. Histopathological analysis of pancreatic islets included assessment of islet lesions, shape (regular *vs.* irregular), islet atrophy, demarcation between islets and exocrine pancreas, and vacuolation and necrosis of islet cells (Azad & Sulaiman, 2020; Gobinath et al., 2022).

2.15. Structure-activity analysis

The correlations between structure and activity were deduced based on ADME-derived parameters, such as electronic/polar [molecular polarizability calculation (MPOL), topological polar surface area (TPSA), molar volume (MOLV), total energy parameter (ETOT)], steric/bulk [molar refractivity (MR)], and hydrophobic (Log P) physiochemical parameters using ADME Works Model Builder software (Fujitsu Kyushu System Engineering Ltd., Version 7.10). Molecular docking simulations were performed using AutoDock 4 (AutoDock Tools v1.5.6). The structure of PIP-1 was designed in ChemSketch 2016.2.2 and converted to MDL Molfiles (V2000), followed by PDB format conversion by OpenBabel GUI 2.4.1. The X-ray crystal structures of COX-2 (PDB ID: 4PH9) and HMGCR (PDB ID: 2R4F) were retrieved from the Protein Data Bank, and subjected to energy minimization using SwissPdbViewer (SPDBV v4.1.0). Prior to docking, ligands, cofactors, and water molecules were removed, and macromolecules were prepared by assigning polar hydrogens, Kollman charges, and atomic solvation parameters. The docking procedure employed genetic and Lamarckian genetic algorithms using Cygwin-I and Cygwin-II. Binding interactions were assessed based on docking scores, binding energies, and RMSD values. Visualization and molecular interaction analysis were conducted using UCSF Chimera 1.11.2.

2.16. Analysis of data

The data were analyzed using SPSS (version 20.0; SPSS Inc., CA) and GraphPad Prism 5 software. Results are presented as mean ± standard error. The normality of the data was assessed using the Shapiro-Wilk test in SPSS (version 20), and the p-value was greater than 0.05, indicating that the data followed a normal distribution. Biochemical analyses and *in vitro* bioactivity studies were evaluated using one-way ANOVA in SPSS, followed by Tukey's post hoc test to determine statistical significance, with experimental triplicates ($n = 3$). *In vivo* acute and chronic studies were analyzed using repeated measures two-way ANOVA in

SPSS, followed by the Least Significant Difference (LSD) test for significance, with six experimental replicates ($n = 6$). Replicate measurements were performed to assess method precision and ensure dataset consistency.

3. Results and discussion

3.1. General

Perna indica (brown mussel), belonging to the family *Mytilidae*, is a rich source of protein and carbohydrates, essential for human nutrition, and is a dietary staple along the southern coast of India. The lipid content analysis has revealed the presence of both beneficial fatty acids and cholesterol, which are important dietary factors (Dalin et al., 2021; Ram et al., 2016). The majority of the carbohydrate content in these mussels consists of pharmacologically potent polysaccharides. Environmental factors, such as water quality and local nutrient availability contribute to the variability in the properties of these polysaccharides, influencing their health benefits (Tan et al., 2023). Research suggests that polysaccharides harvested from certain environments exhibit enhanced bioactive properties compared to those from less favourable ecological conditions (Liu et al., 2018). Mussel polysaccharides have demonstrated efficacy in preventing non-alcoholic fatty liver disease (NAFLD) by modulating the gut microbiota and related gut-liver axis signaling pathways. They also downregulate pro-inflammatory cytokines through the inhibition of the Toll-like receptor 4/nuclear factor kappa B/mitogen-activated protein kinases (TLR4/NF-κB/MAPK) pathway (Wu, Shao, et al., 2019; Liu et al., 2017). These pharmacological effects highlight their potential as anti-inflammatory agents against ulcerative colitis (Xiang et al., 2021). Furthermore, they have been shown to increase short-chain fatty acid (SCFA) levels by modulating intestinal flora, thus activating the phosphoinositide 3-kinase/protein kinase B (PI3K/Akt) signaling pathway and exerting hypoglycemic effects (Wang et al., 2023). This study aims to explore the pharmacological potential of the polysaccharide isolated from *P. indica* collected from the Vizhinjam coast during the February–March season.

3.2. Biochemical analysis and monosaccharide composition of polysaccharide

P. indica yielded 7.3 % crude polysaccharide (PIP) on aqueous extraction followed by ethanol precipitation. PIP contained 70 % total carbohydrate content, 11 % uronic acid content and lesser than 5 % sulfate content (Table 1). Further chromatographic separation (0–0.4 M NaCl) resulted in fractions labeled as PIP-1 to PIP-4 (Fig. S1). Among the four fractions, PIP-1 exhibited the highest carbohydrate content at 72 %, along with 13 % uronic acid and less than 3 % sulfate, making it the most carbohydrate-rich fraction (Table 1). Hence based upon the biochemical parameters and total yield, PIP-1 was selected for detailed spectroscopic analysis, bioactivity assessment, and structure activity correlation. Aqueous extraction followed by ethanol precipitation and anion exchange fractionation are widely used and scalable techniques for polysaccharide isolation, valued for their simplicity, high efficiency, and cost-effectiveness. These methods facilitate polysaccharide recovery and reuse, significantly reducing overall production expenses for nutraceutical purpose (de Freitas et al., 2021). On monosaccharide composition analysis using HPLC system, PIP-1 yielded glucose (54.1 %) and glucuronic acid (45.9 %) (Fig. S2). In a prior study on the monosaccharide composition of mussels, researchers found that polysaccharides extracted using ultrasonic methods predominantly contained glucose (82 %), with uronic acid accounting for 5 %, and the remaining monosaccharides present in amounts below 5 % (Chen et al., 2019). Similarly, 1 → 4 linked polysaccharide from green mussels were reported to have a glucosamine to uronic acid ratio of 3.7:2.6 (Fan et al., 2015).

3.3. Spectroscopic characterization of PIP-1

PIP-1 on spectroscopic investigation was characterized as chain of (1 → 4)-linked-*β*-Glc*p* (glucopyranose) and (1 → 4)-linked-*α*-GlcA*p* (glucopyranuronic acid) (Table 2; Figs. S3-S11). In the FTIR spectrum (Fig. S3), peaks at 3340 cm^{-1} indicated abundant O—H stretching peaks of PIP-1. Symmetric and asymmetric stretching vibration corresponding to skeletal C—H and CH_2 was observed around 2960 cm^{-1}. A sharp peak at 1678 and 1440 cm^{-1} signified asymmetric and symmetric stretching vibration of carboxylate unit of glucopyranuronic acid moiety. Appearance of three peaks at 1140, 1078, and 1035 cm^{-1} confirmed the presence of pyranose ring structure with C-O-C stretching vibrational modes. Multiple bands in 920–840 cm^{-1} represented both *α* and *β* anomers (Hong et al., 2021). The ^{1}H NMR spectrum showed two signals at δ_H 4.50 and 5.08 ppm (Fig. S4), which can be accredited to anomeric peaks of glucopyranose and glucopyranuronic acid moiety. Coupling constant of glucopyranose was greater than 7 Hz and that of glucopyranuronic acid was lesser than 4 Hz, which corresponded *β* and *α* anomers of polysaccharides (Dorst & Widmalm, 2023). Peaks falling between δ_H 3.1 to 3.76 ppm represented pyranoid ring protons (H2-H5) of the PIP-1 subunits (Table 2). ^{13}C NMR spectrum (Fig. S5) at δ_C 95.9 and 92.0 ppm were accredited to the anomeric carbon of glucopyranose and glucopyranuronic acid moiety (Cheng & Neiss, 2012). A downfield peak at δ_C

Table 2
NMR spectroscopic data of (1 → 4)-linked glucuronoglucan PIP-1 from *Perna indica*.

[→4)-*β*-Glc*p*-(1 → 4)-*α*-GlcA*p*-(1→]		
	(1 → 4)-linked-*β*-Glc*p*	(1 → 4)-linked-*α*-GlcA*p*
H_1/C_1	4.50/95.9	5.08/92.0
H_2/C_2	3.10/74.1	3.40/71.4
H_3/C_3	3.34/75.7	3.57/72.8
H_4/C_4	3.27/69.6	3.25/75.9
H_5/C_5	3.58/72.8	3.68/71.5
H_6, H_6'/C_6	3.74,3.76 /60.7	−/−
-COO^-	−/−	−/169.8

Spectral data were acquired on an NMR spectrometer in D_2O as solvent. Chemical shifts (*δ*) were denoted in ppm.

Table 1
Yield and biochemical composition of polysaccharide fractions from *Perna indica*.

Composition[p]	PIP[w]	PIP-1[x]	PIP-2[x]	PIP-3[x]	PIP-4[x]
Yield	7.33	62.33	10.33	9.33	8.55
Total carbohydrate[q]	$69.67^a \pm 0.56$	$72.27^a \pm 1.6$	$29.58^b \pm 2.62$	$21.00^c \pm 2.24$	$19.56^c \pm 1.08$
Uronic acid[q]	$10.78^b \pm 0.55$	$12.74^a \pm 0.59$	$4.59^c \pm 0.41$	$3.87^c \pm 0.58$	$4.59^c \pm 0.65$
Sulfate[q]	$4.66^a \pm 0.58$	$2.54^b \pm 0.58$	$4.15^a \pm 0.16$	$3.88^a \pm 0.20$	$3.85^a \pm 0.26$

The samples were analyzed in triplicate ($n = 3$), and expressed as mean ± standard error.
Means followed by different superscripts (a-c) within the same row indicated significant differences ($p < 0.05$).
[p] Biochemical compositions and yields were expressed as % *w*/w.
[w] PIP is the ethanol precipitate and freeze-dried aqueous polysaccharide concentrate of *P. indica*.
[x] PIP-1 to PIP-4: anion exchange chromatographic fractions eluted with 0–0.4 M NaCl gradients, respectively.
[q] Total carbohydrate, uronic acid, sulfate content (% *w*/w).

169.8 ppm corresponds to the carboxylate group of glucopyranuronic acid moiety. Residual peaks in the range δ_C 60.5–75.9 ppm signified the pyranoid carbons of PIP-1 subunits. Negatively intense peak at δ_C 60.5 ppm in DEPT-135 (Fig. S6) represented methylene carbon of glucopyranose unit (Cheng & Neiss, 2012). HSQC, COSY, and HMBC contour spots were used to establish $^1H—^{13}C$ and $^1H—^1H$ correlations of PIP-1 subunits. Distinctive spots at δ_H/δ_C 4.50/75.9 and 5.08/92.0 ppm in the HSQC spectrum (Fig. S7) represented anomeric correlations. The residual spots were consistent with the data obtained from the ^1H and ^{13}C NMR spectra (Table 2). In the COSY spectrum (Fig. S8), the signals at δ_H/δ_H 4.50/3.10 and 5.08/3.40 ppm corresponded to H1/H2 correlation of PIP-1 subunits. Subsidiary pyranoid ring proton were also established using the COSY spectrum (Fig. S8). HMBC spectrum (Fig. S9) was used to establish interresidual glycosidic linkage. The correlations at $\delta_{C/H}$ 4.50/95.9 and 5.08/69.6 ppm indicate a (1 → 4) glycosidic linkage between the two PIP-1 subunits. Additionally, a correlation was observed between the carboxylate ion and H5 of the glucopyranuronic acid at δ_C/δ_H 169.8/3.68.

Glycosidic linkage analysis of PIP-1 (Fig. S10) was determined using GC–MS fragmentation spectrum of PMAAs, which established (1 → 4) glycosidic linkage patterns. Resultant PMAAs were established as (a) 1,5-diacetoxy-2,3,4,6-tetramethoxy-glucitol (unit A) and (b) 4,5,6-triacetoxy-1,2,3-trimethoxy-glucitol (unit B). GCMS fragmentation spectra exhibited signals corresponding to fragments obtained from the cleavage of bonds. For unit A, base peak at *m/z* 59 represents acetoxy group as most prominent fragment cationic radical. Other peaks at *m/z* 45, 73, 117, 161, and 123, can be accredited to 1° fragments generated as a result of C5-C6, C1-C2, C2-C3, C3-C4 and 2° fragment as result of C3-C4 cleavage. The unit B yielded peaks at *m/z* 45, 59, 133, 217, and 261, which can be associated with the cationic radical ion formed by the cleavage of C1-C2, acetoxy, C3-C4, C4-C3, and C4-C5 (Miao et al., 2014). HR-ESI-MS data analysis of depolymerized PIP-1 (Fig. S11) revealed a a prominent peak at *m/z* 565.3207, corresponding to a decarboxylated [*β*-Glc*p*-(1 → 4)-*α*-GlcA*p*-(1 → 4)-*β*-Glc*p*-(1 → 4)-*α*-GlcA*p*-(1→]$^{4H-}$ fragment. Furthermore, peaks at *m/z* 339.1989 and 311.1671 correspond to the disaccharide [OH-*β*-Glc*p*-(1 → 4)-*α*-GlcA*p*] and decarboxylated form [OH-*β*-Glc*p*-(1 → 4)-*α*-GlcA*p*-OH]$^{H+}$. Based on these observations, PIP-1 was identified as a polymer composed of repeating disaccharide units [→4)-*β*-Glc*p*-(1 → 4)-*α*-GlcA*p*-(1→].

3.4. In vitro pharmacological assessment of PIP and PIP-1

PIP-1 exhibited enhanced antioxidant activity compared to PIP, as evidenced by lower IC_{50} values in DPPH (2 mg/mL), ABTS (7.34 mg/mL), H_2O_2 (1.44 mg/mL) and Fe^{2+} chelation (1.02 mg/mL) assays (Table S1). Conclusively, during fractionation from PIP to PIP-1 there was 8–32 % improvement in IC_{50} values (Table S2). In human body, excess oxidants contribute to the development of non-communicable diseases (NCDs) by increasing oxidative stress, leading to the cellular damage. This imbalance plays a key role in the progression of conditions like diabetes, cardiovascular disease, and neurodegenerative disorders by promoting inflammation, DNA damage, and disruptions in cell signaling pathways (Husain et al., 2023). Polysaccharides, like PIP-1, mitigate oxidative stress through radical scavenging, metal chelation, and the activation of antioxidant enzymes, facilitated by electronegative groups, such as the carboxylate group. By donating electrons, they neutralize free radicals and reactive oxygen species (ROS) while enhancing the activity of antioxidant enzymes like superoxide dismutase (SOD) and glutathione peroxidase (GPx) (Arunachalam et al., 2022). Our study indicated that PIP-1 has moderate antioxidant activity and significant Fe^{2+} chelation ability, comparable to standard antioxidants. This activity is likely due to the hydroxyl and carboxylate groups, which contribute to its radical scavenging properties.

PIP-1 demonstrated a 10 % increase in COX-2 selectivity compared to PIP, with a selectivity index of 1.14 for PIP-1 and 1.04 for PIP (Table S1). PIP-1 exhibited IC_{50} values of 1.09 mg/mL for COX-1 and 0.96 mg/mL for COX-2, whereas PIP showed COX-1 and COX-2 inhibition values exceeding 1 mg/mL (Table S1). In contrast, the standard drug diclofenac sodium displayed a COX-2 selectivity index of 29.34, with IC_{50} values of 48.01 μg/mL for COX-1 and 1.64 μg/mL for COX-2. COXs and 5-LOX are essential enzymes that metabolize arachidonic acid, influencing a range of physiological and pathological processes (Chandrasekharan & Simmons, 2004). COXs facilitate the secretion of prostaglandins and thromboxanes, which are key mediators of inflammation, pain, and fever. COX-1 is constitutively expressed in most tissues, whereas COX-2 is an inducible enzyme primarily upregulated in response to inflammatory stimuli. On the other hand, the enzyme 5-LOX catalyze the synthesis of leukotrienes and hydroperoxy fatty acids from polyunsaturated fatty acids, playing a vital role in the regulation of inflammation and cell signaling pathways (Chandrasekharan & Simmons, 2004; Mashima & Okuyama, 2015). The active site of COX-1 is a long, hydrophobic channel that serves as the binding site for NSAIDs. Compared to COX-2, COX-1 has three amino acid variations. In COX-2, valine at position 523 replaces isoleucine in COX-1, creating an additional side pocket that allows phenylalanine-518 to swing out. Additionally, COX-2 has an arginine in place of histidine-513 in COX-1, enabling interactions with polar moieties (Zarghi & Arfaei, 2011). The NSAIDs with N-pyridine formed proper H-bonding with His90, a crucial key amino acid at the active site. The carbonyl oxygen formed bifurcated H-bonds with Tyr385 and Ser530, whereas the N-hydrazino terminal function enriched the pocket with the donor-acceptor interaction and was held by trifurcated strong H-bonds with Gly526, Ala527, and Ser530 (Abdel-Aziz et al., 2016). Polysaccharides exert their inhibitory effects on COXs and 5-LOX by downregulating the expression of COX-2 and 5-LOX, which in turn reduces the secretion of pro-inflammatory mediators like prostaglandins and leukotrienes. Additionally, they may act by competitively inhibiting the translocation of COX-2 and 5-LOX to their active sites within the cell, thereby hindering their enzymatic activity and contributing to their anti-inflammatory potential (Pedrosa et al., 2023; Kahnt et al., 2022). Molecular docking studies have shown that polysaccharides interact with binding sites similar to those of diclofenac sodium, particularly engaging with Tyr-385 and Ser-530 residues. Their distinct orientation facilitates the chelation of negative charges or electron-rich centers (Utami et al., 2023). Like other polysaccharides, PIP-1 can inhibit 5-LOX activity by chelating the Fe^{2+} cofactor present in the active site of enzyme through its electronegative groups, or by competitively inhibiting the binding of arachidonic acid. PIP-1 may also inhibit 5-LOX-activating protein (FLAP), which is necessary for 5-LOX activation (Aparoy et al., 2012). The high density of polar atoms and electronegative groups in PIP-1 enhance its ability to form hydrogen bonds with key active site residues of 5-LOX and selectively targeted the COX-2 enzyme. Previous studies have shown polysaccharides from marine source with electronegative groups such as carboxylate, and sulfate showed high COX-2 and 5-LOX inhibition efficacy (Pedrosa et al, 2023).

PIP-1 revealed a 10 % elevation in HMGCR inhibition capacity (IC_{50} 0.86 mg/mL) compared to PIP (IC_{50} 0.96 mg/mL) (Table S1). HMGCR serves as the rate-limiting enzyme in the cholesterol biosynthesis pathway, facilitating the conversion of HMG-CoA into mevalonate, which is an essential precursor for cholesterol production (Gesto et al., 2020). Statins competitively bind to the amino acids within the catalytic site of HMGCR, effectively displacing the natural substrate, HMG-CoA. This competitive inhibition decreases the activity of the enzyme, resulting in a reduction in cholesterol synthesis (Murphy et al., 2020). The active site of HMGCR contains binding residues such as Arg-515, Asp-516, Tyr-517, and Asn-518 (Karthik et al., 2012). Polysaccharides can inhibit this enzyme potentially by disrupting its activity or through competitive mechanisms akin to those of statin drugs. Studies suggest that certain polysaccharides may affect the transcriptional regulation of HMGCR and influence protein stability, thereby modulating its enzymatic activity (Wu, Wang, et al., 2019). The hydrophilicity and electronegative groups of PIP-1 can competitively inhibit the binding of the

HMG-CoA substrate, thereby modulating endogenous cholesterol synthesis.

PIP-1 showed negligible elevation (5 %) in ACE inhibition capacity (IC_{50} 3.64 mg/mL) compared to PIP (IC_{50} 3.85 mg/mL) (Table S1). ACE is crucial in the renin-angiotensin-aldosterone system (RAAS), helping regulate blood pressure by inducing vasoconstriction and enhancing sodium retention. ACE catalyzes the conversion of angiotensin I, an inactive precursor, into angiotensin II, a powerful vasoconstrictor. ACE inhibitors reduce blood pressure by lowering angiotensin II levels, which in turn lessens vasoconstriction. Additionally, they increase bradykinin levels, which enhance vasodilation, further contributing to their antihypertensive effects (Lubbe et al., 2020; Arora & Chauhan, 2013; Taddei & Bortolotto, 2016). Shellfish-derived polysaccharides attenuate ACE, hindering the conversion of Angiotensin I to Angiotensin II, which helps regulate systolic and diastolic blood pressure *in vivo*, ultimately reducing hypertension. Additionally, they modulate the production of NO, a vasodilator that influences the contraction and relaxation of vascular smooth muscle cells, contributing to the reduction of hypertension (Xiang et al., 2022). PIP-1 exhibits significantly lower ACE inhibitory activity compared to standard inhibitors such as captopril. Its limited interaction with ACE, suggests that naturally derived PIP-1 is an unlikely candidate for antihypertensive therapy.

PIP-1 showed 8 % decrease in α-amylase inhibition capacity (IC_{50} 3.38 mg/mL) and 11 % elevation in α-glucosidase inhibition (IC_{50} 3.66 mg/mL) compared to PIP (Table S1). The α-Amylase and α-glucosidase are key enzymes involved in carbohydrate digestion, facilitating the breakdown of complex carbohydrates into simple sugars. The α-Amylase specifically hydrolyzes the α bonds in large, α-linked polysaccharides like starch and glycogen, producing shorter chains such as dextrins, maltose, and maltotriose, which are further processed by other enzymes. In contrast, α-glucosidase facilitates the final stage of carbohydrate digestion by hydrolyzing starches and disaccharides into glucose. By cleaving the $(1 \rightarrow 4)$-α linkages in carbohydrates, these enzymes enable glucose absorption through the intestinal lining (Alqahtani et al., 2019). Numerous native polysaccharides derived from marine ecosystems have demonstrated strong α-amylase and α-glucosidase inhibitory effects. This is attributed to functional groups such as sulfate, carboxymethyl, and selenite, which are known to enhance the hypoglycemic properties of polysaccharides, exhibiting IC_{50} values comparable to acarbose (Xue et al., 2023).

Based on the anti-inflammatory and antihypercholesterolemic activity of PIP-1, it was further analyzed in both *in vitro* cell lines and *in vivo* studies. Comparatively lesser activity of PIP-1 against carbohydrate-hydrolyzing enzymes suggested the involvement of alternative pathways for its antidiabetic efficacy; to validate the assumption it was studied in an *in vivo* T1DM model, where carbohydrate-hydrolyzing enzymes play a minimal role.

3.5. PIP-1 modulates NO production in RAW 264.7 macrophages and triglyceride levels in Caco-2 cells

In RAW 264.7 macrophage cells, LPS stimulation resulted in a significant increase in NO production. Treatment with PIP-1 notably reduced NO levels, achieving an IC_{50} of 2.9 μg/mL, while indomethacin required a concentration of 3.8 μg/mL to produce a comparable effect (Table S2). NO acts as a signaling molecule involved in various physiological processes, such as vasodilation, immune responses, and apoptosis regulation. It is synthesized from the amino acid L-arginine by nitric oxide synthases (NOS), with the inducible form (*i*NOS) being primarily responsible for high-output NO production during inflammation. Under normal conditions, NO has anti-inflammatory properties by inhibiting the recruitment of inflammatory cells. However, excessive NO production can contribute to tissue damage and aggravate inflammation by promoting the release of pro-inflammatory cytokines (Sharma et al., 2007). Due to its significant roles in inflammation, NO serves not only as a biomarker of disease activity but also as a key target for therapeutic interventions. Glucans and their derivatives have been shown to modulate *i*NOS mRNA expression in a concentration-dependent manner when macrophages are activated by LPS (Lee et al., 2009). The activation of pathogen recognition receptors (PRRs) plays a crucial role in regulating iNOS levels in macrophages, indicating that this pathway is central to the anti-inflammatory effects of such polysaccharides (Wold et al., 2024). Similarly, PIP-1 may help mitigate excessive NO production by modulating the *i*NOS pathway.

After a 4-day incubation, Caco-2 cells exhibited hyperlipidemic triglyceride levels (1.77 mg/dL). Administration of PIP-1 (0.1–160 μg/dL) led to a concentration-dependent reduction in triglyceride levels (8–54 %) ($p < 0.05$). In comparison, atorvastatin (10 μM) resulted in an 89 % reduction in elevated triglyceride levels (Table S2). Caco-2 cells, a commonly used human intestinal epithelial cell line, provide valuable insights into lipid absorption mechanisms and the effects of therapeutic agents. Their ability to form tight junctions and exhibit polarized morphology makes them ideal for studying lipid metabolism under controlled conditions (Hiebl et al., 2020). When Caco-2 cells are exposed to fatty acids and glycerol, the fatty acids are esterified with glycerol-3-phosphate to form triglycerides. This process is facilitated by diacylglycerol acyltransferase (DGAT), which catalyzes the final step of converting diacylglycerol and fatty acyl-CoA into triglycerides (Alves-Bezerra & Cohen, 2017). Once synthesized, triglycerides are incorporated into lipoproteins, primarily chylomicrons and very low-density lipoproteins (VLDL), for transport through the bloodstream by complex internal and external signaling pathways that regulate lipid metabolism and energy storage (Alves-Bezerra & Cohen, 2017). Previous studies on hypolipidemic polysaccharides have shown their positive effects in reducing fatty acid absorption and inhibiting triglyceride and cholesterol synthesis (Zhan et al., 2021). In our study, atorvastatin significantly reduced triglyceride levels, demonstrating its effectiveness in promoting lipid clearance and modulating lipid metabolism (Aslani et al., 2023). The inhibitory effects of PIP-1 may be attributed to its ability to regulate lipid absorption and triglyceride synthesis, similar to the effects observed with other native polysaccharides.

3.6. Acute oral toxicity studies of PIP-1 in Swiss albino mice and SD rats

In this study, rats and mice administered with 300 and 2000 mg/kg b. wt. of PIP-1 showed no mortality over the 14-day observation period. PIP-1 at both doses showed no pathological lesions or mortality among the studied animals. No notable physical or behavioural changes were observed in either species during this time. In mice, key organs such as the heart, spleen, kidneys, and liver exhibited a decrease in relative body weight index, which was within the permissible limit. Conversely, organs such as the reproductive system, adrenal glands, lungs, and brain showed an increase in relative body weight index which was within the permissible limit. Similarly, in rats, the heart and lungs showed a decrease in relative body weight index which was within the permissible limit, while other organs demonstrated an increase in relative body weight index (Fig. S12). Additionally, toxicity studies indicated that the LD_{50} of PIP-1 exceeded 2000 mg/kg b. wt. Acute toxicity studies, conducted by monitoring the effects of test samples on rats and mice in controlled environments, are essential for assessing potential toxicity levels. These studies provide crucial insights that help determine the safe use of substances in humans and other organisms (Chorawala et al., 2013). A non-toxic sample shows negligible change in relative organ weight and no alterations in both physiological and behavioural patterns of animals (Aamir et al., 2021). As per the OECD guideline AOT 420, histopathological evaluation was not deemed necessary, as no gross pathological lesions or macroscopic abnormalities were observed in the organs. However, future studies should include comprehensive histopathological assessments of all the organs to detect subclinical tissue damage and further validate the safety profile of PIP-1 at therapeutic doses. The dosage of PIP-1 was determined based on its LD_{50} value and the conversion of the human equivalent dose (HED) to the animal

equivalent dose (AED) (Nair & Jacob, 2016).

3.7. PIP-1 reduced paw edema induced by carrageenan and formalin

In the acute inflammation study (30 min to 5 h) following carrageenan administration, a rapid increase in paw thickness was observed, which was linked to vascular dilation, moderate inflammatory cell infiltration, severe epidermal vacuolation, and edema in the dermis, along with moderate subcutaneous inflammatory cell infiltration (Table 3; Fig. 1A & 1B). Mice treated with PIP-1 at both doses exhibited moderate anti-inflammatory response during the early phase (30 min to 2 h). The lower and higher doses of PIP-1 resulted in a 1.2- and 1.5-fold increase in paw edema inhibition, respectively, during the early phase, while indomethacin demonstrated a 1.7-fold increase (Table 3; Fig. 1A). In the late phase (3–5 h), the higher dose of PIP-1 was more effective in reducing paw edema, showing a 1.6-fold improvement compared to 1.3-fold for the lower dose and 1.4-fold for indomethacin (Fig. 1A). Treatment with PIP-1, at either dose, showed negligible variation in studied parameters . Both the treatments showed mild inflammatory cell infiltration and moderate edema in dermis, while the epidermal vacuolation was mild in low dose and minimum in high dose (Fig. 1C & 1D). In contrast, the indomethacin-treated group showed mild inflammatory cell infiltration in the dermis and subcutaneous tissue, accompanied by a slight reduction in dermal edema and epidermal vacuolation (Fig. 1E).

In the chronic inflammation study (1 to 10 days) following formalin administration, there was a steady increase in paw thickness (Fig. 1F). During the neurogenic phase of inflammation (day 1–3), PIP-1 at both doses demonstrated higher inhibition of paw thickness compared to indomethacin. As the days progressed from 1 to 3, PIP-1 at both low and high doses showed approximately 2-fold increase in paw edema inhibition, while indomethacin showed negligible variations in initial phase (Table 3; Fig. 1F). During the transition from the neurogenic phase to the sustained inflammatory phase (day 3-4), the extent of inhibition in the PIP-1 treated group dropped by approximately 7-fold for the lower dose and 2-fold for the higher dose, while indomethacin showed no change in inhibition. As the sustained inflammatory phase progressed (day 4-10), PIP-1 at both doses increased its inhibition efficacy by 8-fold and 4-fold (at lower and higher doses, respectively), reaching 47 % and 76 % by the end of day 10 (Table 3; Fig. 1F). However, indomethacin showed a 3-fold increase in inhibition, reaching 92 % by day 10 (Fig. 1F). Histopathological analysis of paw tissues from mice across the different treatment groups further supported the anti-inflammatory effects (Fig. 1G-1J). Formalin treatment led to marked inflammatory cell infiltration in the dermis and subcutaneous tissue, epidermal necrosis with scab formation, and mild to moderate edema in the dermis (Fig. 1G). The lower dose of PIP-1 showed little variation in these parameters (Fig. 2H), whereas the higher dose reduced dermal edema, epidermal necrosis, and scab formation to a minimum (Fig. 1I). Indomethacin restored the epidermal architecture with apparently normal epidermis and reducing inflammatory cell infiltration in the dermis and subcutaneous tissues to minimum (Fig. 1J).

The carrageenan-and formalin-induced paw edema model is widely regarded as an effective tool for simulating acute and chronic inflammation, often used by researchers to explore inflammatory mechanisms and assess the therapeutic potential of novel agents (Ajayi et al., 2021). Swiss albino mice are widely used for investigating inflammatory responses due to their well-characterized immune systems and genetic similarity to humans. The key differences that impact how inflammation is initiated, sustained, and resolved are the cytokine profiles, TLR signaling pathways, and immune cell populations (Bjornson-Hooper et al., 2022; Vaure & Liu, 2014). Additionally, the mechanisms underlying the inflammatory cascade in rodents, particularly in paw edema models, may not fully replicate human chronic inflammatory conditions. For example, while COX-2 inhibition plays a significant role in both species, the relative contribution of prostaglandins, leukotrienes, and NO differs between rodents and humans, potentially affecting drug efficacy comparisons (Henriques et al., 1987). Carrageenan-induced edema model is characterized by a biphasic inflammatory response. The early phase, occurring within the first 2 h post-carrageenan injection, is driven by histamine and serotonin, leading to increased vascular permeability, significant neutrophil infiltration, and initial edema (Patil et al., 2019). The neutrophil infiltration triggers the release of reactive oxygen species, NO and peroxynitrite which modulate the inflammation in early phase (Morris, 2003). The late phase, emerging between 3 and 5

Table 3
Anti-inflammatory impacts of PIP-1 and indomethacin in carrageenan- and formalin-induced Swiss albino mice for acute and chronic studies.

Acute anti-inflammatory study using carrageenan-induced paw edema							
Time (h)	Carrageenan (CAR)	CAR+ indomethacin (10 mg/kg b.wt.)		CAR+ PIP-1(22 mg/kg b. wt.)		CAR+ PIP-1 (110 mg/kg b. wt.)	
	Change in paw volume (mm)	Change in paw volume (mm)	Extent of inhibition (%)	Change in paw volume (mm)	Extent of inhibition (%)	Change in paw volume (mm)	Extent of inhibition (%)
0.5	0.65 ± 0.07^{Ab}	0.37 ± 0.07^{CDa}	43.08	0.36 ± 0.04^{ABa}	44.61	0.4 ± 0.03^{Ba}	38.46
1	1.09 ± 0.08^{Deb}	0.55 ± 0.09^{Da}	49.54	0.43 ± 0.06^{ABCa}	60.55	0.58 ± 0.09^{Ba}	46.79
2	1.25 ± 0.06^{Eb}	0.34 ± 0.09^{BCDa}	72.80	0.57 ± 0.07^{Ca}	54.40	0.52 ± 0.09^{Ba}	58.40
3	1.07 ± 0.04^{CDc}	0.23 ± 0.03^{ACa}	66.14	0.48 ± 0.05^{BCb}	55.14	0.46 ± 0.1^{Bb}	57.01
4	$1.05 \pm 0.08B^{CDc}$	0.18 ± 0.01^{ABa}	82.86	0.42 ± 0.03^{BCb}	60.00	0.39 ± 0.1^{Bab}	62.86
5	0.89 ± 0.04^{BDc}	0.07 ± 0.02^{Aa}	92.13	0.24 ± 0.03^{Ab}	73.03	0.08 ± 0.01^{Aa}	91.01
Chronic anti-inflammatory study using formalin-induced paw edema							
Days	**Formalin (FOR)**	**FOR+ indomethacin (10 mg/kg b.wt.)**		**FOR+ PIP-1(22 mg/kg b. wt.)**		**FOR+ PIP-1 (110 mg/kg b. wt.)**	
	Change in paw volume (mm)	**Change in paw volume (mm)**	**Extent of inhibition (%)**	**Change in paw volume (mm)**	**Extent of inhibition (%)**	**Change in paw volume (mm)**	**Extent of inhibition (%)**
Day 1	1.19 ± 0.06^{Ba}	0.85 ± 0.03^{Aefg}	28.57	0.97 ± 0.05^{Ac}	18.49	0.95 ± 0.02^{Ade}	20.17
Day 2	1.39 ± 0.11^{Bb}	0.94 ± 0.15^{Afg}	32.37	0.86 ± 0.05^{Abc}	38.13	0.83 ± 0.06^{Acde}	40.28
Day 3	1.3 ± 0.11^{Ba}	0.88 ± 0.14^{Aeg}	32.31	0.78 ± 0.05^{Aac}	40.00	0.75 ± 0.05^{Abd}	42.30
Day 4	1.93 ± 0.10^{Cef}	1.33 ± 0.10^{Ah}	31.09	1.82 ± 0.12^{BCfg}	5.70	1.54 ± 0.12^{ABh}	20.21
Day 5	1.97 ± 0.09^{Cf}	1.28 ± 0.08^{Ah}	35.02	1.83 ± 0.16^{BCg}	7.11	1.52 ± 0.05^{ABgh}	22.84
Day 6	1.09 ± 0.13^{Ag}	1.09 ± 0.13^{Ag}	0	1.68 ± 0.19^{BCef}	< 0	1.38 ± 0.04^{ABfh}	< 0
Day 7	1.74 ± 0.13^{Cce}	0.81 ± 0.11^{Adef}	53.45	1.53 ± 0.16^{BCd}	12.07	1.16 ± 0.02^{ABe}	33.33
Day 8	1.69 ± 0.12^{Bbc}	0.60 ± 0.13^{Ace}	64.50	1.52 ± 0.16^{Bde}	10.06	0.87 ± 0.05^{Ad}	48.52
Day 9	1.66 ± 0.13^{Bbc}	0.46 ± 0.08^{Ab}	72.29	1.41 ± 0.16^{Bd}	15.06	0.59 ± 0.11^{Abc}	64.46
Day 10	1.58 ± 0.12^{Cbc}	0.12 ± 0.02^{Aa}	92.40	0.83 ± 0.14^{Babc}	47.47	0.37 ± 0.03^{Aa}	76.58

b. wt.*- Body weight.
The samples were analyzed (n = 6), and expressed as mean ± standard error.
Means followed by different superscripts (a-h) within the same column indicated significant differences ($p < 0.05$).
Means followed by different superscripts (A-D) within the same row indicated significant differences ($p < 0.05$).

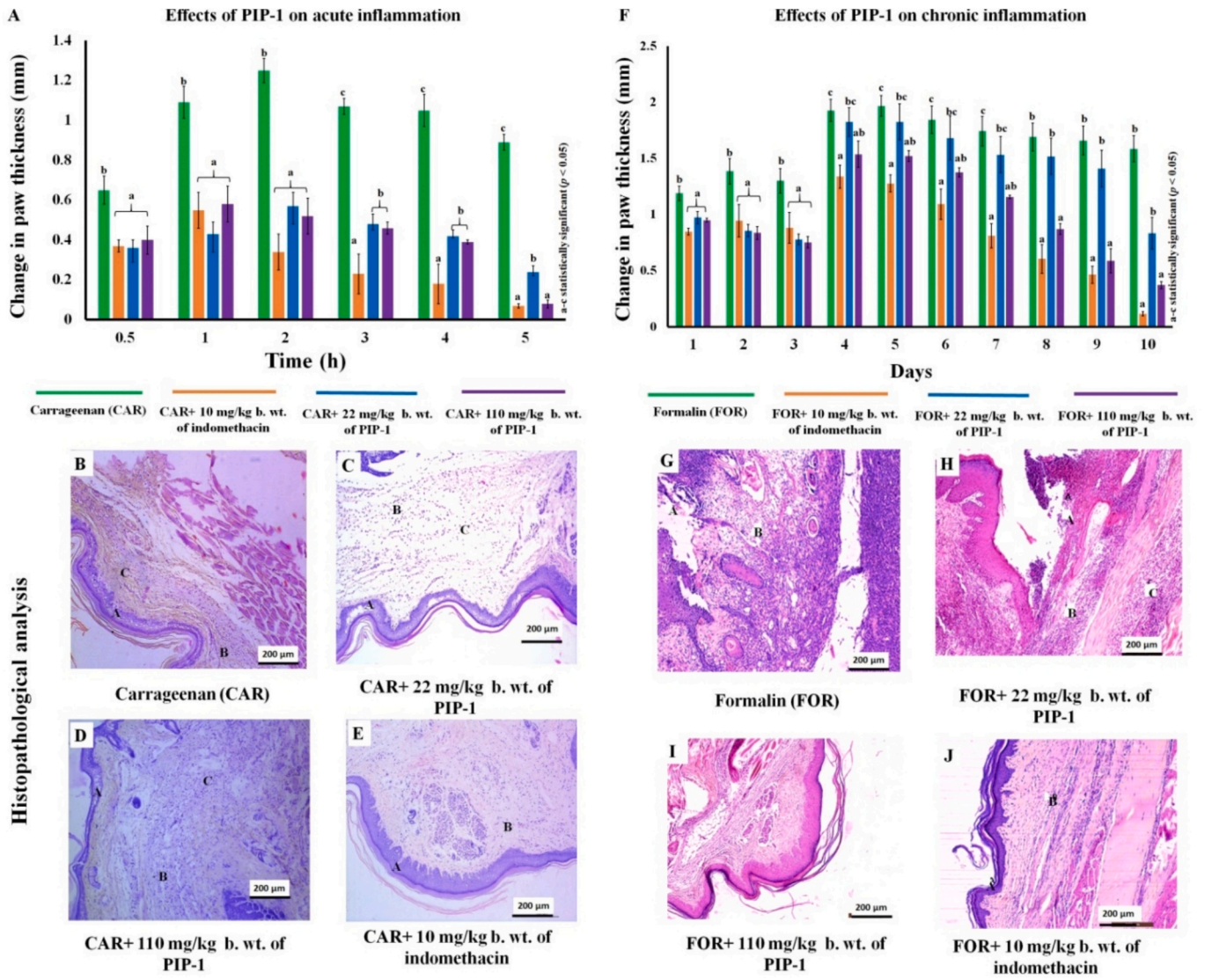

Fig. 1. (A) Changes in paw thickness of Swiss albino mice following carrageenan induction over a 5 h period. (B, C, D, & E) Histopathology of paw tissues (H&E, X100). Area represented as A, B & C in histopathological images signifies epidermal vacuolation, inflammatory cell infiltration and edema in dermis across respective treatment. (F) Changes in paw thickness of Swiss albino mice following formalin induction over a 10-day period. (G, H, I, & J) Histopathology of paw tissues (H&E, X100). Area represented as A, B & C in histopathological images signifies changes in epidermal cells, inflammatory cell infiltration in dermis and subcutaneous tissues across respective treatment groups.

h after injection, involves the release of inflammatory mediators such as bradykinin, NO, prostaglandins, and cytokines like IL-1β and IL-6 (Patil et al., 2019; Loram et al., 2007). Conventional treatments for managing the early phase of inflammation typically include antihistamines and corticosteroids, which help to reduce vasodilation and histamine release. In the later phase of inflammation, NSAIDs are commonly used to inhibit cyclooxygenase enzymes, reducing prostaglandin production and controlling inflammation (Ali et al., 2023). Corticosteroids modulate epidermal, dermal, and leukocyte functions in inflammatory skin diseases by binding to cytoplasmic receptors, forming a steroid-receptor complex that alters gene transcription and inhibits the synthesis of specific pro-inflammatory proteins (Ramamoorthy & Cidlowski, 2016). In contrast, H1-antihistamines reduce inflammation by blocking histamine from binding to H1 receptors, thereby inhibiting biological effects of histamine (Tatarkiewicz et al., 2019). NSAIDs inhibit COX-2 enzyme activity thereby reducing the production of prostaglandins. Reduction of prostaglandin level in turn reduce the secretion of cytokines (Park et al., 2006). Similarly, formalin-induced paw edema acts through biphasic defence mechanism. Acute phase or neurogenic phase mediated by secretion of neuropeptides such as substance P and calcitonin gene-related peptide (CGRP) on activation of Transient Receptor Potential Ankyrin 1 (TRPA1) by formalin. These mediators are involved in neurogenic inflammation and vasodilation, promoting increased vascular permeability and leading to edema formation (Demartini et al., 2022; McNamara et al., 2007). Unlike neurogenic phase which shows direct nociceptive response, Phase II or sustained inflammatory phase involves complex inflammatory cascade involving variety of inflammatory substances, including prostaglandins, serotonin, histamine, bradykinin, NO and cytokines, such as IL-1β (Arzi et al., 2015). In carrageenan- and formalin-induced paw edema, agonists modulate inflammatory pathways through toll-like receptors (TLR2/6 and TLR4) (Myers et al., 2019). In carrageenan-induced models, the primary focus is on inhibiting COX enzymes and reducing pro-inflammatory cytokines, while in formalin-induced models, the emphasis shifts towards modulating nociceptive signaling and preventing central sensitization. In both models, PIP-1 effectively reduced paw thickness, showing a more pronounced effect during the late phase, comparable to the anti-inflammatory effects of indomethacin. This suggested that PIP-1

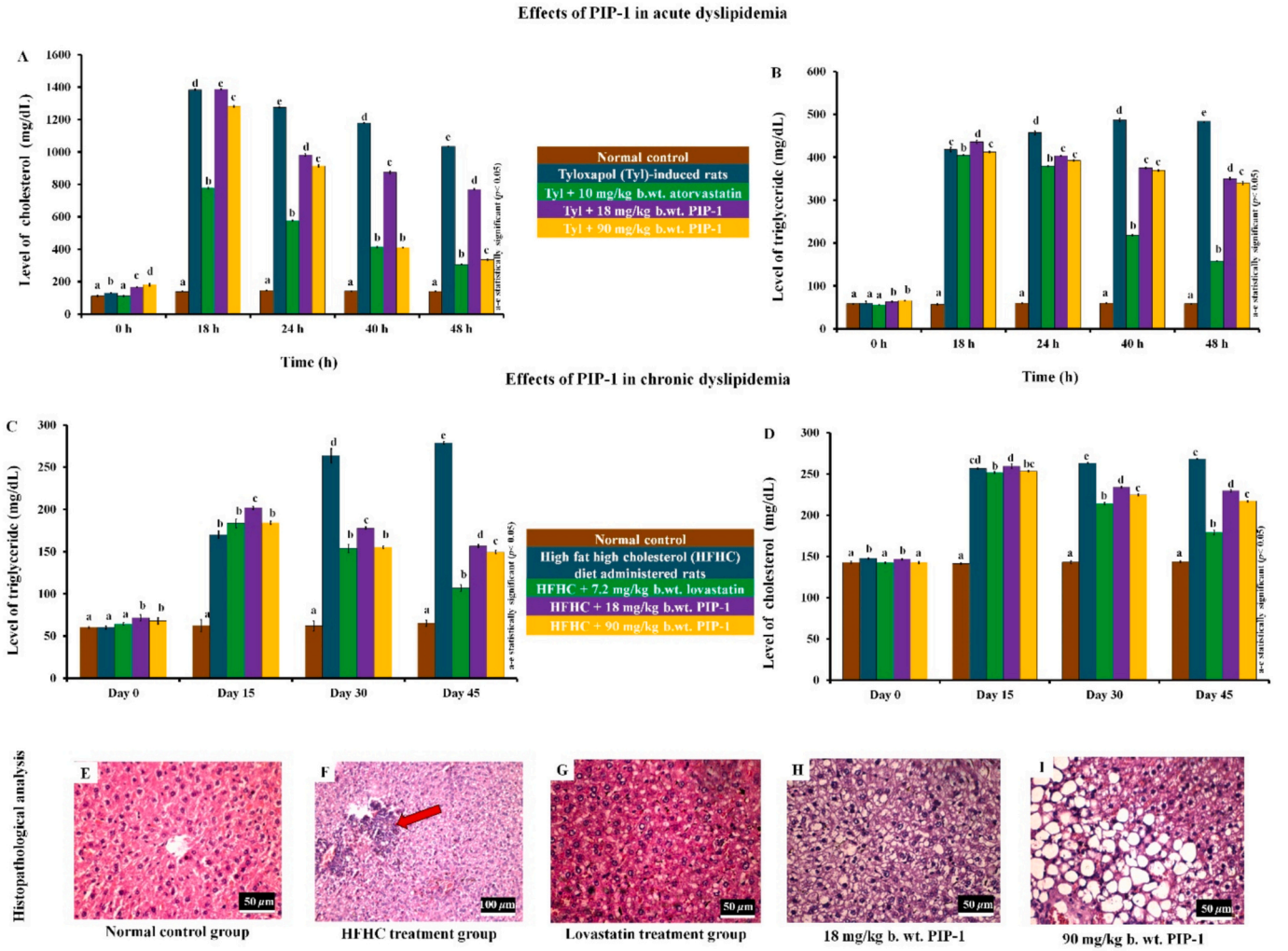

Fig. 2. (A & B) Variation in level of cholesterol and triglyceride in SD rats induced with tyloxapol during 48 h study period. (C & D) Variation in level of triglyceride and cholesterol in SD rats administered with HFHC diet during 45-day study period. (E) Liver - Normal architecture of liver with cords of hepatocytes radiating away from central vein (H&E, X400) (F) Severe microvesicular steatosis and foci of mononuclear cell infiltration (arrow) (H&E, X200) in sham group (G) Hepatocytes showing mild microvesicular steatosis (H&E, X400) in lovastatin treatment group (H, I) Hepatocytes with severe steatosis (H&E, X400) in low and high dosage treatment groups of PIP-1.

has potential in modulating NO, cytokines, prostaglandins, and other inflammatory mediators, supporting earlier *in vitro* findings. The superior activity of PIP-1, at both doses, during the neurogenic phase of formalin-induced paw edema demonstrated higher inhibition than indomethacin, indicating its potential in inhibiting neuropeptides or TRPA1 activation. Polysaccharides similar to PIP-1 can interact with TLR4 through their electronegative groups to modulate inflammation (Hsu et al., 2024). Their hydrophilic nature makes them well-suited for interacting with surface receptors on cells involved in inflammatory pathways (Huo et al., 2025). In conclusion, PIP-1 shows mild efficacy in modulating nociceptive signaling pathways and strong efficacy in inhibiting the inflammatory cascade and central sensitization. Previous paw edema study of ulvan from *Ulva fasciata* reported 65 % inhibition of carrageenan-induced paw edema and 70 % inhibition of formalin-induced paw edema (Govindan & Thomas, 2021), which were lower than the 91 % and 76 % inhibition observed in the PIP-1-treated group, respectively. Polysaccharides from the *Mytilidae* family has shown their ability to regulate inflammatory cytokines such as TNF-α, IL-6, and IL-10 by inhibiting the NF-κB signaling pathway (Xiang et al., 2021). Similarly, sulfated glucans have demonstrated the ability to suppress iNOS and COX-2 expression, which are responsible for producing key inflammatory cytokines (Hou et al., 2020).

3.8. PIP-1 modulated triglyceride and cholesterol level in blood plasma of SD rats

In the 48-h acute dyslipidemia study, normal rats displayed no notable variations in TC or TG levels. However, following the administration of tyloxapol (400 mg/kg b. wt.), there was an intense 8-fold increase in both TG and TC levels within 48 h (Table 4; Fig. 2A & 2B). Rats receiving a high dose of PIP-1 experienced a steady decline in TC levels over the 48 h period, ultimately reaching about 68 %, similar to the atorvastatin-treated group (~71 %) ($p < 0.05$) (Fig. 2A). On the other hand, the low-dose PIP-1 group showed no significant variation in TC levels after 24 h (~25 %) (Fig. 2A). Both PIP-1 doses resulted in approximately 25 % reduction in TG levels, while atorvastatin produced a 55 % reduction (Fig. 2B). In 45-day chronic dyslipidemia study was assessed by administrating HFHC diet in rats. Over the period of 45 days, TC and TG levels increased by 2 and 4-folds (Table 4; Fig. 2C &2D). Rats administered with high dose of PIP-1 showed approximately 19 % and 46 % decrease in TC and TG levels whereas lovastatin standard showed 33 % and 62 %, respectively (Fig. 2C & 2D) ($p < 0.05$). Similarly, low dose of PIP-1 showed approximately 14 % and 43 % decrease in TC and TG levels (Fig. 2C &2D). Microscopic analysis of liver sections from animals fed a normal diet revealed well-preserved liver architecture,

Table 4
Antidyslipidemic effects on triglyceride and cholesterol levels in acute and chronic hyperlipidemic rat models.

Level of cholesterol (mg/dL) in acute condition					
Treatments	0 h	18 h	24 h	40 h	48 h
Normal control	111.98 ± 3.78^{Aa}	139.14 ± 2.5^{Ab}	145.98 ± 1.36^{Ab}	142.3 ± 2.07^{Ab}	140.7 ± 2.58^{Ab}
Tyloxapol	131.28 ± 2.88^{Ba}	1383.26 ± 3.74^{Ce}	1275.51 ± 3.08^{Ed}	1179.14 ± 2.77^{Dc}	1034.8 ± 1.61^{Eb}
Tyloxapol +10 mg/kg b. wt. * of atorvastatin	111.68 ± 2.23^{Aa}	779.29 ± 4.73^{Be}	576.7 ± 4.05^{Bd}	415.17 ± 4.26^{Bc}	305.38 ± 1.24^{Bb}
Tyloxapol +18 mg/kg b. wt. of PIP-1	165.85 ± 1.51^{Ca}	1387.36 ± 3.49^{De}	980.76 ± 8.45^{Dd}	874.34 ± 7.87^{Cc}	770.48 ± 4.03^{Db}
Tyloxapol +90 mg/kg b. wt. of PIP-1	181.52 ± 8.02^{Da}	1282.04 ± 5.28^{Ee}	914.64 ± 8.29^{Cd}	411.8 ± 2.05^{Bc}	335.38 ± 5.66^{Cb}
Level of triglyceride (mg/dL) in acute condition					
Treatments	**0 h**	**18 h**	**24 h**	**40 h**	**48 h**
Normal control	58.61 ± 0.94^{Aa}	56.88 ± 1.73^{Aa}	59.72 ± 0.93^{Aa}	60.04 ± 0.44^{Aa}	58.45 ± 0.48^{Aa}
Tyloxapol	59.61 ± 0.93^{Aa}	417.98 ± 4.66^{Cb}	456.91 ± 4.77^{Dc}	487.16 ± 4.23^{Dd}	484.14 ± 3.02^{Ed}
Tyloxapol +10 mg/kg b. wt. of atorvastatin	55.92 ± 1.65^{Aa}	404.66 ± 1.74^{Be}	379.26 ± 3.62^{Bd}	218.39 ± 1.75^{Bc}	158.06 ± 3.64^{Bb}
Tyloxapol +18 mg/kg b. wt. of PIP-1	63.82 ± 1.22^{Ba}	435.98 ± 4.26^{De}	403.03 ± 0.68^{Cd}	374.88 ± 1.58^{Cc}	350.04 ± 2.54^{Db}
Tyloxapol +90 mg/kg b. wt. of PIP-1	65.98 ± 1.41^{Ba}	412.48 ± 1.04B^{Ce}	392.59 ± 1.57^{Cd}	369.68 ± 1.77^{Cc}	340.17 ± 3.95^{Cb}
Level of cholesterol (mg/dL) in chronic condition					
Treatments	**0th day**	**15th day**	**30th day**	**45th day**	
Normal control	142.63 ± 1.14^{Aa}	141.27 ± 0.97^{Aa}	142.93 ± 1.49^{Aa}	143.39 ± 1.26^{Aa}	
HFHC diet administered rats	147.57 ± 0.72^{Ab}	256.39 ± 0.48^{Bcd}	263.18 ± 0.55^{Ce}	268.17 ± 0.47^{De}	
HFHC diet + Lovastatin (7.2 mg/kg b. wt.)	142.42 ± 0.66^{Aa}	251.61 ± 1.042^{Db}	214.08 ± 1.00^{Cb}	179.20 ± 2.94^{Bb}	
HFHC diet + PIP-1 (18 mg/kg b. wt.)	146.47 ± 0.72^{Ab}	259.36 ± 2.53^{Dd}	233.83 ± 1.12^{Cd}	229.57 ± 1.20^{Bd}	
HFHC diet + PIP-1 (90 mg/kg b. wt.)	142.44 ± 1.22^{Aa}	253.35 ± 0.78^{Dbc}	224.56 ± 0.98^{Cc}	216.79 ± 0.66^{Bc}	
Level of triglyceride (mg/dL) in chronic condition					
Treatments	**0th day**	**15th day**	**30th day**	**45th day**	
Normal control	60.41 ± 1.06^{Aa}	62.37 ± 1.14^{Aa}	62.06 ± 1.47^{Aa}	65.13 ± 1.97^{Aa}	
HFHC diet administered rats	60.07 ± 0.97^{Aa}	170.12 ± 6.95^{Bb}	263.50 ± 6.11^{Cd}	278.74 ± 3.58^{Dd}	
HFHC diet + Lovastatin (7.2 mg/kg b. wt.)	64.38 ± 1.66^{Aa}	183.66 ± 4.50^{Db}	153.8 ± 8.43^{Cb}	106.70 ± 1.52^{Bb}	
HFHC diet + PIP-1 (18 mg/kg b. wt.)	71.70 ± 1.56^{Ab}	201.99 ± 5.29^{Dc}	177.66 ± 4.86^{Cc}	156.62 ± 4.188^{Bc}	
HFHC diet + PIP-1 (90 mg/kg b. wt.)	67.91 ± 3.52^{Ab}	184.25 ± 1.89^{Db}	155.41 ± 1.43^{Cb}	149.45 ± 2.09^{Bc}	

b. wt.*- Body weight.
The samples were analyzed (n = 6), and expressed as mean ± standard error.
Means followed by different superscripts (a-e) within the same row indicated significant differences ($p < 0.05$).
Means followed by different superscripts (A-E) within the same column row indicated significant differences ($p < 0.05$).

with hepatocyte cords radiating from the central vein. The hepatocytes had abundant cytoplasm, distinct nuclei, and clear sinusoidal spaces between the cords (Fig. 2E). The heart and kidneys also appeared histologically normal. In contrast, untreated animals exhibited severe microvesicular steatosis, covering over 80 % of the liver tissue, along with moderate infiltration of mononuclear inflammatory cells, though ballooning degeneration was minimal (Fig. 2F). The heart displayed minimal fatty changes, but no lesions were seen in the kidneys. Hyperlipidemic rats showed liver inflammation, steatosis, and mild ballooning degeneration. In PIP-1 treated groups, no lesions were found in the kidneys or heart at either doses. The liver showed minimal lobular inflammation and no ballooning degeneration, but hepatocytes exhibited severe steatosis, with higher doses leading to both micro- and macrovesicular steatosis (Fig. 2H & 2I). Lovastatin-treated rats demonstrated improved parameters, with liver sections showing only mild microvesicular steatosis, minimal inflammation, and no ballooning degeneration (Fig. 2G).

Tyloxapol-induced hyperlipidemia and hypercholesterolemia have been widely studied for their effects on lipid metabolism, offering profound insights into lipid disorders. Following tyloxapol induction, total triglyceride (TG), total cholesterol (TC), very low-density lipoprotein cholesterol (VLDL-C), low-density lipoprotein cholesterol (LDL-C), and phospholipid levels increase, while high-density lipoprotein cholesterol (HDL-C) decreases (Akinmoladun et al., 2021). Tyloxapol acts as a potent inhibitor of lipoprotein lipase (LPL), the enzyme responsible for hydrolyzing triglycerides in lipoproteins. By inhibiting LPL, tyloxapol prevents triglyceride uptake, leading to the accumulation of triglyceride-rich lipoproteins in blood plasma, thereby disrupting normal lipoprotein metabolism and resulting in elevated lipid levels in the bloodstream (Drug Bank Online, 2024). Additionally, they elevate blood cholesterol levels by stimulating cholesterol production in the liver through increased HMGCR activity and by decreasing the clearance of LDL-C (Huynh et al., 2024). High-fat diet-fed SD rats are commonly used to study drug effects on dyslipidemia and cardiovascular issues, as they show increased LDL, decreased HDL, and cardiac changes like mononuclear cell infiltration and perivascular fat accumulation, contributing to vascular dysfunction (Udomkasemsab & Prangthip, 2019). They modify the lipid profile by upregulating enzymes involved in lipid synthesis and downregulating the clearance of lipoproteins in lipid metabolism pathways (Zhukova et al., 2014). The tyloxapol model highlighted the effect of PIP-1 on lipid regulation under conditions of endogenous lipid metabolism dysfunction. Since LPL inhibition and increased HMGCR activity disrupt lipid homeostasis, this model is useful in assessing influence of PIP-1 on triglyceride and cholesterol levels in the presence of dysregulated LPL and HMGCR activity. In contrast, the high-fat, high-cholesterol diet model simulates conditions in which exogenous lipids are introduced through diet, representing lifestyle-related metabolic disorders. Here, lipid metabolism involves both endogenous synthesis and dietary lipid intake, affecting overall lipid regulation. Thus, both models provide a comprehensive evaluation of effects of PIP-1 on dyslipidemic conditions, and the observed variations in triglyceride and cholesterol levels can be attributed to differences in metabolic pathways governing lipid homeostasis in these two models. Mediterranean diet has been shown to lower Apo B concentrations, suggesting dietary interventions can play a role in managing cardiovascular risk (Lamantia et al., 2016). Polysaccharides exert their antiyslipidemic effects by inhibiting the absorption of dietary lipids, influencing lipid transport, suppressing endogenous cholesterol synthesis, and promoting cholesterol metabolism. Additionally, they act through antioxidant mechanisms, modulation of gut microbiota, regulation of pro-inflammatory cytokines, and activation of AMPK signaling pathways (Jing et al., 2022). In both tyloxapol-induced and HFHC diet-fed rats, elevated levels of TC and TG were observed. In the tyloxapol-induced model, PIP-1 may inhibit the synthesis of TC and TG, promote TC metabolism, improve lipid transport, reduce pro-inflammatory cytokine expression, and modulate the AMPK signaling pathway in the

short term. However, in the longer-term study with HFHC diet-fed rats, PIP-1 demonstrated a greater effect on TG modulation compared to TC, suggesting it more effectively influences the synthesis and metabolism of TG over TC. Effects of PIP-1 are dependent on its ability to inhibit key enzymes like HMGCR, fatty acid synthase, and acetyl-CoA carboxylase, as well as receptors such as apolipoprotein B (Apo B) and sterol regulatory element-binding proteins (SREBP). Previous studies on polysaccharides from *Nitraria retusa* showed reductions in total cholesterol and triglycerides comparable to PIP-1 in the tyloxapol-induced dyslipidemia model (Rjeibi et al., 2019). Similarly, ulvan from *Ulva pertusa* reduced total cholesterol by 17.6 % and triglycerides by 33.5 %, which was lower than the 19 % and 46 % reductions observed with PIP-1 (Jiang et al., 2020). This inhibition is likely mediated by van der Waals interactions between the carboxylate and hydroxyl groups of PIP-1 and these targets. These results are consistent with earlier research on marine polysaccharides. For instance, polygalactofucans from *Sargassum spp.* reduced triglyceride levels by enhancing LPL activity in high-fat diet-induced rats (Chakraborty & Maneesh, 2020). Similarly, sulfated polysaccharides from *Phascolosoma esculenta* exhibited hepatoprotective and hypolipidemic effects by modulating the atherogenic index, liver index, and antioxidant levels (Wu et al., 2020). Polysaccharides from *Chlorella pyrenoidosa* and *Ostrea rivularis* activate the AMPK pathway, enhancing HMGCR phosphorylation and regulating SREBP-1c, thereby influencing lipid metabolism and gut microbiota (Kong et al., 2021; Wan et al., 2019). Additionally, mussel polysaccharides exhibit anti-inflammatory effects, coupled with positive impacts on intestinal flora, which help modulate long-term conditions such as obesity, diabetes mellitus, and inflammatory bowel disease (Xiang et al., 2021). Tyloxapol-induced and HFHC diet-induced dyslipidemia models in rats effectively replicate key aspects of human dyslipidemia. Consequently, these models can contribute to conditions that simulate cardiovascular disease risk factors observed in human populations (Mallya & Lewis, 2024). However, the lipid metabolism differs substantially between rats and humans, impacting the translational relevance of rodent studies to human physiology and disease (Panzoldo et al., 2011).

3.9. Acute effects of PIP-1 on glucose level of SD rats

Normal rats exhibited minimal variation in plasma glucose levels during the 5 h study period, with only a 12 % fluctuation (Table 5). Administration of PIP-1 at a dose of 270 mg/kg b. wt. resulted in a 7–18 % reduction in glucose levels during the 5 h study period, while metformin at 500 mg/kg b. wt. led to a decrease of 4–10 %. This model is used to screen effects of hypoglycemic agent in animals. Here PIP-1 showed reduction in blood glucose level within physiological level and was comparable with standard drug metformin, which indicated possible hypoglycemic effect in normal rats (El Hilaly & Lyoussi, 2002).

Table 5
Variation in level of glucose in normal SD rats over 5 h study period.

Treatment	Normal control	Metformin (500 mg/kg b. wt.)		PIP-1 (270 mg/kg b. wt.)	
	Level of glucose (mg/dL)	Level of glucose (mg/dL)	Variation in glucose level (%)	Level of glucose (mg/dL)	Variation in glucose level (%)
0 h	135.33 ± 3.44^{Bb}	122.33 ± 4.82^{BCa}	9.60	110.33 ± 2.80^{Aa}	18.47
1 h	118.5 ± 4.84^{Aa}	113.333 ± 2.28^{Aab}	4.36	105.5 ± 3.34^{Aa}	10.97
2 h	118.5 ± 2.12^{Ab}	106.67 ± 3.83^{Aa}	9.98	109.5 ± 3.23^{Aab}	7.59
3 h	136.33 ± 3.44^{Bb}	123.33 ± 4.82^{Ca}	9.53	111.33 ± 2.80^{Aa}	18.33
4 h	119.5 ± 4.84^{Ab}	114.33 ± 2.28^{ABab}	4.33	106.5 ± 3.34^{Aa}	10.87
5 h	119.5 ± 2.12^{Ab}	107.67 ± 3.827^{Aa}	9.90	110.5 ± 3.23^{Aab}	7.53

b. wt.- Body weight.
The samples were analyzed (n = 6), and expressed as mean ± standard error.
Means followed by different superscripts (a-b) within the same row indicated significant differences ($p < 0.05$).
Means followed by different superscripts (A-C) within the same column indicated significant differences ($p < 0.05$).

3.10. Acute and chronic impacts of PIP-1 on STZ-induced Swiss albino rats

Normal rats exhibited no change in glucose levels during the 5 h study period (Table 6). However, following intraperitoneal injection of STZ, blood glucose levels increased 2.8-fold, resulting in hyperglycemia (Fig. 3). PIP-1, at either dosage, failed to significantly reduce the STZ-induced glucose elevation. At the higher dose, PIP-1 lowered glucose levels by 15 %, while the lower dose achieved a 6 % reduction by the end of 5 h. In contrast, metformin caused a 46 % increase in glucose levels. Although metformin showed a steady improvement in reducing glucose levels over time, PIP-1 exhibited only minimal progress as the study progressed. In chronic study, normal rats showed little to no variation in glucose level (5 %) during 21-day study period. On administration of STZ, blood glucose levels increased 2–3 fold, resulting in prolonged hyperglycemia (Fig. 3). PIP-1, at either dose showed no hypoglycemic activity. As study progress there was decrease in glucose inhibition efficiency of PIP-1 leading to no effect on day 21. However, metformin showed increase in glucose inhibition efficacy as study progress to reach 44 % inhibition at end of study period (Table 6; Fig. 3). Histopathological analysis also supported the above observation (Fig. 3C-3G). Microscopic examination of pancreas from normal control rats showed normal architecture of islets with aggregates of small, round to polygonal cells. The islets were regular and roughly round in shape and islet cells showed moderate to abundant cytoplasm and round to oval nucleus. There was clear demarcation between the islets and the exocrine pancreas (Fig. 3C). In STZ-induced rats, more than 75 % of the islets in the sections showed lesions such as mild to moderate necrosis and mild vacuolation. There was reduction in the size of the islets and multifocal loss of clear demarcation between endocrine and exocrine pancreas (Fig. 3D). Even though, the lesions such as necrosis and vacuolation showed a diffuse distribution in the group of rats that received standard treatment, there was a reduction in the degree of severity. The islets showed minimum necrosis and vacuolation. Atrophy of islets was minimal and the restoration of islet size was evident (Fig. 3E). In the PIP-1 low dosage group there was presence of lesions in most of the islets, mild to moderate vacuolation and mild necrosis of islet cells. Demarcation between islets and exocrine pancreas was indistinct at multiple foci. Islets showed minimal to marked atrophy and many islets had irregular shape (Fig. 3F). Treatment with high dose of PIP-1 revealed reduction in the severity of lesions when compared to lower dose. Vacuolation in the islet cells was mild, while the necrosis of cells was minimal to mild. There was loss of demarcation between endocrine and exocrine pancreas at multiple foci. Though some islets showed irregular shape, there was no reduction in the size of the islets and was comparable to the size of the islets in vehicle control group (Fig. 3G).

STZ specifically targets and destroys insulin-producing beta cells in the pancreas of both neonatal and adult rats, resulting in hyperglycemia and diabetes mellitus. This property makes STZ an effective tool for modeling and studying the pathophysiology of T1DM in experimental settings (Baig & Panchal, 2020). STZ triggers an increase in inflammatory cytokines and ROS, leading to immune cell infiltration, oxidative stress, mitochondrial dysfunction, and β-cell apoptosis (Bathina & Das, 2021). This autoimmune-driven inflammatory environment exacerbates β-cell destruction and impairs glucose regulation, worsening diabetes (Shen et al., 2022). Additionally, STZ alkylates DNA, causing damage that activates apoptosis pathways, further compromising β-cell function and insulin regulation (Zhu, 2022). The resulting insulin deficiency disrupts glucose homeostasis, a hallmark of T1DM, allowing researchers

Table 6
Acute and chronic effects of PIP-1 in STZ-induced SD rats.

Acute effects of PIP-1 in STZ-induced SD rats								
Time (h)	Normal control	Diabetic control (STZ)	STZ + Metformin (50 mg/kg b.wt.)		STZ + PIP-1 (90 mg/kg b.wt.)		STZ + PIP-1 (270 mg/kg b.wt.)	
	Level of glucose (mg/dL)	Level of glucose (mg/dL)	Level of glucose (mg/dL)	Variation in glucose level (%)	Level of glucose (mg/dL)	Variation in glucose level (%)	Level of glucose (mg/dL)	Variation in glucose level (%)
0	132.2 ± 0.33^{Aa}	376.8 ± 1.11^{Bc}	377.4 ± 4.26^{Bf}	< 0	371.6 ± 4.09^{Bf}	1.38	372.6 ± 3.57^{Bf}	1.27
1	131 ± 0.75^{Aa}	373.2 ± 1.15^{Dbc}	304.8 ± 1.86^{Be}	18.30	365.4 ± 3.71^{Ce}	2.09	363.2 ± 4.36^{Ce}	2.67
2	130.8 ± 1.71^{Aa}	370 ± 0.75^{Dab}	268.8 ± 4.43^{Bd}	27.30	357.6 ± 3.79^{Cd}	3.35	355 ± 4.67^{Cd}	4.05
3	131.4 ± 1.34^{Aa}	367.6 ± 0.78^{Da}	211 ± 1.9^{Bc}	42.60	350.4 ± 3.85^{Cc}	4.68	343.4 ± 3.26^{Cc}	6.58
4	130.4 ± 1.12^{Aa}	365.2 ± 0.91^{Ea}	200 ± 3.56^{Bb}	45.23	343.8 ± 4.03^{Db}	5.86	315.2 ± 2.72^{Cb}	13.69
5	127.2 ± 1.58^{Aa}	362.8 ± 0.87^{Ea}	195 ± 1.94^{Ba}	46.25	340 ± 3.99^{Da}	6.28	306.6 ± 2.62^{Ca}	15.49
Chronic effects of PIP-1 in STZ-induced SD rats								
Days	**Normal control**	**Diabetic control (STZ)**	**STZ + Metformin (50 mg/kg b.wt.)**		**STZ + PIP-1 (18 mg/kg b.wt.)**		**STZ + PIP-1 (90 mg/kg b.wt.)**	
	Level of glucose (mg/dL)	**Level of glucose (mg/dL)**	**Level of glucose (mg/dL)**	**Variation in glucose level (%)**	**Level of glucose (mg/dL)**	**Variation in glucose level (%)**	**Level of glucose (mg/dL)**	**Variation in glucose level (%)**
Day 0	120.5 ± 0.391^{Aa}	357.83 ± 1.588^{Dd}	231.33 ± 5.738^{Bd}	35.35	303 ± 1.509^{Cd}	15.32	298 ± 1.509^{Cd}	16.72
Day 7	122.83 ± 1.517^{Aa}	305 ± 1.269^{Ec}	198 ± 1.202^{Bc}	35.08	296.33 ± 1.326^{Dc}	2.84	288 ± 1.509^{Cc}	5.57
Day 14	122.5 ± 0.612^{Aa}	293.33 ± 2.535^{Db}	186.33 ± 1.305^{Bb}	36.47	292.33 ± 1.326^{Db}	0.34	282 ± 1.394^{Cb}	3.86
Day 21	127.17 ± 0.549^{Aa}	282.17 ± 4.419^{CDa}	156.5 ± 1.867^{Ba}	44.54	287 ± 1.581^{Da}	< 0	275.33 ± 1.347^{Ca}	2.52

b. wt.- Body weight.
The samples were analyzed (n = 6), and expressed as mean ± standard error.
Means followed by different superscripts (a-f) within the same coloumn indicated significant differences ($p < 0.05$).
Means followed by different superscripts (A-E) within the same row indicated significant differences ($p < 0.05$).

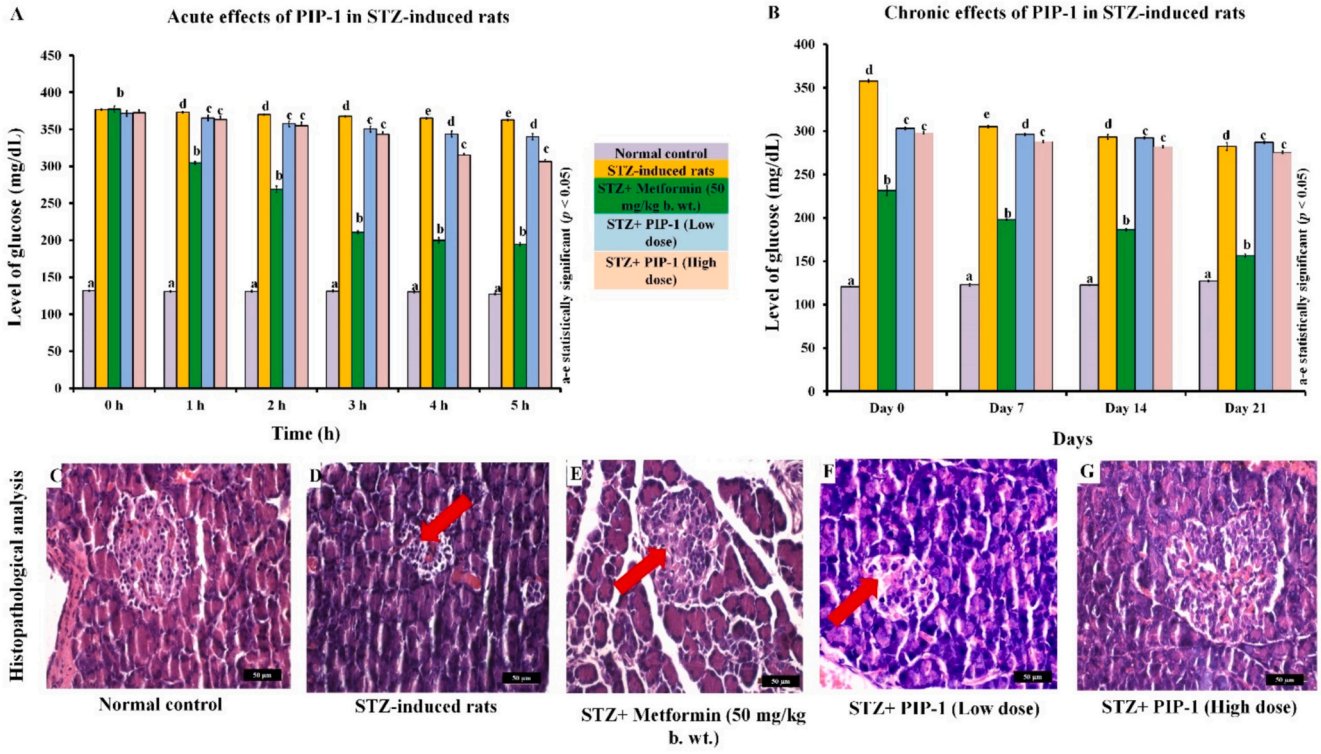

Fig. 3. (A & B) Variation in glucose levels in streptozotocin induced rats in acute and chronic conditions (C) Normal control group with pancreas islets with normal architecture (H & E, X400). (D) Hyperglycemic group with atrophied islets (arrow) with decreased number of β-cells and presence of vacuolation (H & E, X400). (E) Metformin treated group with restored islets (arrow) with increase in number of β-cells and reduction in vacuolation (H & E, X400). (F) Low dose PIP-1 treated group with markedly atrophied islet with reduced number of islet cells and islet cell necrosis (arrow) (H&E, X400). (G) High dose PIP-1 treated group with moderate improvement in β-cell density and mild vacuolation (H & E, X400).

to explore interventions to preserve β-cell function (Zhu, 2022). Polysaccharides demonstrate hypoglycemic effects by promoting the repair of islet β-cells, regulating enzyme activity, reducing oxidative stress, alleviating inflammation, and modifying the composition of gut microbiota. (Zhang, Lu, Li, & Song, 2025). Previous studies have shown that polysaccharides derived from the Asian clam and pacific oyster possess hypoglycemic properties by regulating carbolytic enzymes, boosting the activity of antioxidant enzymes such as glutathione peroxidase (GSH-Px), catalase (CAT), and superoxide dismutase (SOD) and reducing malondialdehyde (MDA) levels. Additionally, they modulate the phosphoinositide 3-kinase/protein kinase B (PI3K/AKT) signaling pathway (Getachew et al., 2019; Wang et al., 2019). Similarly, certain native polysaccharides prevent islet cell apoptosis and stimulate insulin secretion by upregulating the expression of specific proteins and mRNA involved in these processes (Zhang et al., 2014). Furthermore, some polysaccharides alleviate T1DM by promoting the anti-inflammatory factors production and reduce the expression of pro-inflammatory factors (Wang et al., 2020). In this study, PIP-1 exhibited minimal to no hypoglycemic activity under both acute and chronic conditions, which may be attributed to the absence of functional groups like sulfate, phosphate, acetyl, carboxymethyl, alkyl, and selenite that are known to enhance the hypoglycemic effects of polysaccharides (Zhang, Zeng, et al., 2025). However, the presence of hydroxyl groups on PIP-1 presents opportunities for future research aimed at improving its bioactivity through targeted functional group modifications.

3.11. Structure-activity relationship of PIP-1

PIP-1 disaccharide unit on ADME analysis yielded ADME physicochemical parameters with a favourable value (Table S3). The molecular descriptors for PIP-1 suggest that it has hydrophilic properties, indicated by a low log *P* value of −3.35, making it more soluble in water. Its electronic parameters, such as MPOL (29.22) and TPSA (209.43), reflect its ability to interact with biological targets, particularly through hydrogen bonding, given the high number of hydrogen bond acceptors (NUMHBA: 12) and donors (NUMHBD: 7). Sterically, PIP-1 exhibits flexibility (FLXBRC: 12) and moderate molecular volume (MOLV: 87.08). These characteristics suggest potential efficacy as a therapeutic agent, especially for aqueous environments. MPOL and TPSA values, combined with significant hydrophilic nature and hydrogen bonding capacity, highlight strong polar nature and potential of PIP-1 for robust interactions. The high density of polar atoms enhances its ability to form hydrogen bonds with biological targets, such as receptors or enzymes. This characteristic facilitates binding, making PIP-1 suitable for therapeutic applications where strong receptor-ligand interactions are crucial (Bunally et al., 2019; Press Books, 2023; Durrant Lab, 2024).

In the molecular docking studies, the number of hydrogen bonds formed between PIP-1 and the target proteins was 4, for COX-2 and 5, for HMGCR, contributing to binding stability. The binding energy values were − 9 kcal/mol for COX-2 and -8.74 kcal/mol for HMGCR, while the docking scores were − 10.1 kcal/mol and − 8.99 kcal/mol, respectively, indicating a stronger predicted binding affinity for COX-2. The inhibition constant (Ki) was lower for COX-2 (252.40 nM) compared to HMGCR (390.28 nM), suggesting higher inhibitory potency. Additionally, intermolecular energy values were − 10.19 kcal/mol (COX-2) and − 9.91 kcal/mol (HMGCR), while the torsional free energy remained constant at 1.19 kcal/mol for both complexes (Fig. S13; Table S4). The stronger anti-inflammatory potential of PIP-1, compared to its anti-dyslipidemic activity, was confirmed through *in silico* studies, which align with the experimental findings.

The biological activities of polysaccharides are strongly influenced by their structural attributes, including functional groups, glycosidic linkages, and branching degree (Wang et al., 2022). The functional groups like sulfate, carboxylate and phosphate can influence charge, polarity and size thus directly impacting molecular binding efficacy. Charged groups generally bind more strongly than polar groups, which in turn bind more effectively than nonpolar functional groups. Studies on polysaccharide containing glucuronic acid functional group revealed potent anti-inflammatory activity reducing expression of NO, TNF-α and IL-6 by modulating TLR4/MyD88/NF-κB signaling pathway (Gao et al., 2024). Similarly, uronic containing polysaccharide ameliorates intestinal inflammation in mice by inhibiting the TLR4/JNK signaling pathway. They can upregulate the expression of ZO-1 and Occludin mRNA, which are important for maintaining the intestinal barrier function (Zhang, Zeng, et al., 2025). These uronic acids containing polysaccharide shows antidyslipidemic activity can influence intestinal microflora of mice and its treatment markedly increased mRNA expression of cholesterol 7α-hydroxylase (CYP7A1) and bile salt export pump (BSEP), suggesting an enhancement of bile acids (BAs) synthesis and excretion in liver (Guo et al., 2020). Previous reports on (1 → 3) and (1 → 4) linked uronic acid containing polysaccharide have broad spectrum of bioactivity, especially lipid regulatory activity (Ji et al., 2023). Polysaccharide primarily built in with (1 → 4) has shown their ability to reduce NO and pro-inflammatory cytokines production through the phosphorylation inhibition of MAPK signal pathway (Huo et al., 2025). The degree of branching in polysaccharides plays a crucial role in determining their biological activity by influencing molecular weight and structural conformation. Previous research suggests that polysaccharides with a lower branching degree tend to exhibit enhanced immune-stimulating properties. This indicates a potential optimal branching degree for maximum bioactivity. Excessive branching may reduce water solubility, while insufficient branching could limit available binding sites, thereby affecting overall functionality (Wang et al., 2022).

4. Conclusions

Perna indica sourced from southwest coast of India is recognized not only as a nutritious delicacy but also as a promising source of pharmacological potential in the fight against chronic ailments. This dual benefit emphasize the importance of incorporating *P. indica* into dietary practices, not only for its culinary appeal but also for its potential contributions to public health. The polysaccharide derived from *P. indica* possess significant pharmacological potential, highlighting their role in promoting health and combating chronic diseases. In the present study, the (1 → 4)-linked glucuronoglucan composed of repeating β-D-glucose (Glc*p*) and α-D-glucuronic acid (GlcA*p*) units isolated from *P. indica* (PIP-1) showed prominent anti-inflammatory and anti-dyslipidemic activity by inhibiting enzymes such as COXs, 5-LOX and HMGCR. *In vitro* experiments revealed that PIP-1 decreased NO secretion in LPS-stimulated macrophages and reduced triglyceride levels in Caco-2 cells. These effects can be attributed to ability of PIP-1 to modulate macrophage signaling pathways and triglyceride metabolism by interacting with the active sites of receptors and enzymes through its electronegative groups. In carrageenan- and formalin-induced paw edema models, PIP-1 (at a higher dose) significantly reduced paw thickness, closely resembling the effects observed in the standard indomethacin group, highlighting its ability to modulate inflammatory markers associated with paw edema. Similarly, in both acute and chronic *in vivo* dyslipidemia models, PIP-1 (at a higher dose) moderately decreased triglyceride and cholesterol levels, similar to the effects of statin drugs. Histopathological studies further demonstrated improvements in paw and liver tissues throughout the study period. These findings support the role of the functional groups in PIP-1 in regulating physicochemical properties, which favourably modulate inflammation and lipid metabolism pathways. Integrating polysaccharide extraction along with mussel mariculture presents a viable and cost-effective strategy, enhancing the value of aquaculture while promoting a sustainable supply. Overall, these findings proposed that PIP-1 could hold promise as a functional food, offering potential applications in the treatment of chronic inflammation and dyslipidemia related disorders. Future studies will focus on developing a nutraceutical formulation and assessing its long-term safety profile through

accelerated shelf-life studies, as well as chronic and subchronic toxicity evaluations.

CRediT authorship contribution statement

Ashwin A. Pai: Writing – review & editing, Writing – original draft, Visualization, Validation, Software, Methodology, Investigation, Formal analysis, Data curation. **Kajal Chakraborty:** Writing – review & editing, Writing – original draft, Validation, Supervision, Resources, Project administration, Investigation, Funding acquisition, Data curation, Conceptualization. **Archana Raj:** Writing – review & editing, Validation, Software, Methodology, Investigation, Formal analysis, Data curation. **Bibu John Kariyil:** Writing – review & editing, Validation, Supervision, Resources, Project administration, Formal analysis, Data curation. **Shubhajit Dhara:** Writing – review & editing, Visualization, Methodology, Formal analysis, Data curation. **R. Anoopraj:** Methodology, Formal analysis, Data curation.

Ethical approval

All applicable international, national, and/or institutional guidelines for the care and use of animals were followed. The study was approved by the Institutional Animal Ethical Committee, College of Veterinary and Animal Sciences, Thrissur, Kerala, with sanction order no. sanction order numbers CVAS/MTY/IAEC/23/36 dated 15/3/2023, CVAS/MTY/IAEC/23/37 dated 15/3/2023 and CVAS/MTY/IAEC/23/51 dt. 13/09/2023.

Declaration of competing interest

The authors declare that they have no known competing financial interests or personal relationships that could have appeared to influence the work reported in this paper.

Acknowledgements

The authors gratefully acknowledge the funding by the Indian Council of Agricultural Research (ICAR, New Delhi, India)-funded National Agriculture Science Fund (NASF) of the ICAR, New Delhi, India (Grant No. NASF-ICAR/CMFRI/9-1965/2022-23). The authors are grateful to the Director, of ICAR-CMFRI, Chairperson, Department of Chemistry, Mangalore University, and the University officials of Kerala Veterinary and Animal Sciences University for facilitating the research activities. The authors are grateful to SAIF, IIT Madras, and SCS, MG University, Kottayam, Kerala, India for providing the spectroscopic data. The authors are also grateful to the Dean, College of Veterinary and Animal Sciences, Mannuthy for the support extended for the smooth conduct of research.

Appendix A. Supplementary data

Supplementary data to this article can be found online at https://doi.org/10.1016/j.foodres.2025.116397.

Data availability

Data will be made available on request.

References

Aamir, K., Sugumar, V., Khan, H. U., Looi, C. Y., Juneja, R., Waqas, M., & Arya, A. (2021). Non-toxic nature of chebulinic acid on biochemical, hematological, and histopathological analysis in normal Sprague Dawley rats. *Toxicological Research, 38*(2), 159–174. https://doi.org/10.1007/s43188-021-00092-3

Abdallah, E. E., Abd-Elhady, A. A., & Elsaid, M. Y. (2015). Effect of atorvastatin (ATOR) on the cardiac muscle fibres in hyperlipidemic adult male albino rats (structural and biochemical study). *The Egyptian Journal of Hospital Medicine, 58*(1), 143–166. https://doi.org/10.21608/ejhm.2015.15525

Abdel-Aziz, A. A. M., Abou-Zeid, L. A., ElTahir, K. E. H., Ayyad, R. R., El-Sayed, M. A. A., & ElAzab, A. S. (2016). Synthesis, anti-inflammatory, analgesic, COX-1/2 inhibitory activities and molecular docking studies of substituted 2-mercapto-4(3H)-quinazolinones. *European Journal of Medicinal Chemistry, 121*, 410–421. https://doi.org/10.1016/j.ejmech.2016.05.066

Ajayi, A. M., Alabi, A. O., Oyibo, A. O., & Joseph, O. O. (2021). Antioedematogenic and anti-inflammatory actions of *Phragmanthera incana* (Schum) Balle leaf in carrageenan-induced inflammation models in rats. *Advances in Traditional Medicine, 21*, 701–711. https://doi.org/10.1007/s13596-020-00480-4

Akinmoladun, A. C., Adegbamigbe, A. D., Okafor, N. R., Josiah, S. S., & Olaleye, M. T. (2021). Toxicological and pharmacological assessment of a multiherbal phytopharmaceutical on Triton X-1339-induced hyperlipidemia and allied biochemical dysfunctions. *Journal of Food Biochemistry, 45(3), Article 13238*. https://doi.org/10.1111/jfbc.13238

Ali, K. A., Maity, A., Roy, S. D., Pramanik, S. D., Das, P. P., & Shaharyar, M. A. (2023). Insight into the mechanism of steroidal and non-steroidal anti-inflammatory drugs. In I. Kazmi, S. Karmakar, M. A. Shaharyar, M. Afzal, & F. A. Al-Abbasi (Eds.), *How synthetic drugs work* (pp. 61–94). Elsevier Inc.

Alqahtani, A. S., Hidayathulla, S., Rehman, M. T., ElGamal, A. A., Al-Massarani, S., Razmovski-Naumovski, V., … AlAjmi, M. F. (2019). Alpha-amylase and alpha-glucosidase enzyme inhibition and antioxidant potential of 3-oxolupenal and katononic acid isolated from *Nuxia oppositifolia*. *Biomolecules, 10*(1), Article 61. https://doi.org/10.1007/s13596-020-00480-4

Alves-Bezerra, M., & Cohen, D. E. (2017). Triglyceride metabolism in the liver. *Comprehensive Physiology, 8*(1), 1–8. https://doi.org/10.1002/cphy.c170012

Aparoy, P., Reddy, K. K., & Reddanna, P. (2012). Structure and ligand based drug design strategies in the development of novel 5- LOX inhibitors. *Current Medicinal Chemistry, 19*(22), 3763–3778. https://doi.org/10.2174/092986712801661112

Appukuttan, K. K., & Nair, T. P. (1983). Culture of the brown mussel *Perna indica* at Vizhinjam, southwest coast of India. *Proceedings of the Symposium on Coastal Aquaculture, 2*, 526–533.

Appukuttan, K. K., Nair, T. P., & Thomas, K. T. (1989). Spat settlement of brown mussel *Perna indica* Kuriakose and Nair in the southwest coast of India. *Journal of the Marine Biological Association of India, 31*(1&2), 266–275.

Arora, P. K., & Chauhan, A. (2013). ACE inhibitors: A comprehensive review. *International Journal of Pharmaceutical Sciences and Research, 4*(2), 532–548.

Arunachalam, K., Sreeja, P. S., & Yang, X. (2022). The antioxidant properties of mushroom polysaccharides can potentially mitigate oxidative stress, beta-cell dysfunction, and insulin resistance. *Frontiers in Pharmacology., 13, Article 874474*. https://doi.org/10.3389/fphar.2022.874474

Arzi, A., Olapour, S., Yaghooti, H., & Karampour, N. S. (2015). Effect of royal jelly on formalin-induced inflammation in rat hind paw. *Jundishapur Journal of Natural Pharmaceutical Products, 10(1), Article 22466*. https://doi.org/10.17795/jjnpp-22466

Aslani, S., Razi, B., Imani, D., Mohammadi, K., Jamialahmadi, T., Reiner, Z., & Sahebkar, A. (2023). Effect of statins on the blood lipid profile in patients with different cardiovascular diseases: A systematic review with meta-analysis of randomized clinical trials. *Current Medicinal Chemistry, 30*(32), 3702–3724. https://doi.org/10.2174/0929867330666221129094921

Azad, A. K., & Sulaiman, W. M. A. W. (2020). Antidiabetic effects of *P. Macrocarpa* ethanolic fruit extract in streptozotocin-induced diabetic rats. *Future. Journal of Pharmaceutical Sciences, 6*(1), Article 57. https://doi.org/10.1186/s43094-020-00073-7

Baig, M. A., & Panchal, S. S. (2020). Streptozotocin-induced diabetes mellitus in neonatal rats: An insight into its applications to induce diabetic complications. *Current Diabetes Reviews, 16*(1), 26–39. https://doi.org/10.2174/1573399815666190411115829

Bathina, S., & Das, U. N. (2021). *Resolvin D1 decreases the severity of streptozotocin-induced type 1 diabetes mellitus by enhancing BDNF levels, reducing oxidative stress, and suppressing inflammation. International journal of molecular sciences, 22(4), Article 1516*. https://doi.org/10.3390/ijms22041516

Benalaya, I., Alves, G., Lopes, J., & Silva, L. R. (2024). *A review of natural polysaccharides: Sources, characteristics, properties, food, and pharmaceutical applications. International journal of molecular sciences, 25(2), Article 1322*. https://doi.org/10.3390/ijms25021322

Bi, S., Jing, Y., Cui, X., Gong, Y., Zhang, J., Feng, X., Shi, Z., Zheng, Q., & Li, D. (2024). A novel polysaccharide isolated from *Coriolus versicolor* polarizes M2 macrophages into an M1 phenotype and reverses its immunosuppressive effect on the tumor microenvironment. *International Journal of Biological Macromolecules, 259(2), Article 129352*. https://doi.org/10.1016/j.ijbiomac.2024.129352

Bjornson-Hooper, Z. B., Fragiadakis, G. K., Spitzer, M. H., Chen, H., Madhireddy, D., Hu, K., … Nolan, G. P. (2022). A comprehensive atlas of immunological differences between humans mice, and non-human primates. *Frontiers in immunology, 13, Article 867015*. https://doi.org/10.3389/fimmu.2022.867015

Press Books. (2023). *Topological polar surface area*. Retrieved from https://pressbooks.openeducationalberta.ca/abcofpkpd/chapter/tpsa/. Accessed October 10, 2024.

Budreviciute, A., Damiati, S., Sabir, D. K., Onder, K., Schuller-Goetzburg, P., Plakys, G., … Kodzius, R. (2020). Management and prevention strategies for non-communicable diseases (NCDs) and their risk factors. *Frontiers in Public Health, 8, Article 574111*. https://doi.org/10.3389/fpubh.2020.574111

Bunally, S. B., Luscombe, C. N., & Young, R. J. (2019). Using physicochemical measurements to influence better compound design. *SLAS Discovery: Advancing Life Sciences R&D, 24*(8), 791–801. https://doi.org/10.1177/2472555219859845

Chakraborty, K., & Joy, M. (2020). High-value compounds from the molluscs of marine and estuarine ecosystems as prospective functional food ingredients: An overview. *Food Research International, 137, Article 109637*. https://doi.org/10.1016/j.foodres.2020.109637

Chakraborty, K., & Maneesh, A. (2020). Marine-derived polygalactofucan and its *β*-2-deoxy-amino-substituted glucopyranan composite attenuate 3-hydroxy-3-methyl-glutaryl-CoA reductase: Prospective natural anti-dyslipidemic leads. *Medicinal Chemistry Research, 29*, 281–300. https://doi.org/10.1007/s00044-019-02482-7

Chandrasekharan, N. V., & Simmons, D. L. (2004). The cyclooxygenases. *Genome Biology, 5(9), Article 241*. https://doi.org/10.1186/gb-2004-5-9-241

Chen, W., Jia, Z., Zhu, J., Zou, Y., Huang, G., & Hong, Y. (2019). Optimization of ultrasonic-assisted enzymatic extraction of polysaccharides from thick-shell mussel (*Mytilus coruscus*) and their antioxidant activities. *International Journal of Biological Macromolecules, 140*, 1116–1125. https://doi.org/10.1016/j.ijbiomac.2019.08.136

Cheng, H. N., & Neiss, T. G. (2012). Solution NMR spectroscopy of food polysaccharides. *Polymer Reviews, 52*(2), 81–114. https://doi.org/10.1080/15583724.2012.668154

Chorawala, M. R., Trivedi, V. R., Dave, D. J., Oza, P. M., & Shah, G. B. (2013). Acute and subacute toxicity studies of cell wall contents of probiotic (*lactobacillus casei*) in Wistar rats and Swiss albino mice. *Research Journal of Pharmaceutical, Biological and Chemical Sciences, 4*(2), 719–732.

Dalin, M., Saritha, K., & Patterson, J. (2021). Lipid and fatty acid profile variations in *Perna indica* and *Perna viridis* of Kanyakumari district, southeast and southwest coast of India. *Iranian Journal of Fisheries Sciences, 20*(3), 761–772. https://doi.org/10.22092/ijfs.2021.124066

Demartini, C., Greco, R., Magni, G., Zanaboni, A. M., Riboldi, B., Francavilla, M., … Tassorelli, C. (2022). Modulation of glia activation by TRPA1 antagonism in preclinical models of migraine. *International Journal of Molecular Sciences, 23(22), Article 14085*. https://doi.org/10.3390/ijms232214085

Dorst, K. M., & Widmalm, G. (2023). NMR chemical shift prediction and structural elucidation of linker-containing oligo- and polysaccharides using the computer program CASPER. *Carbohydrate Research, 533, Article 108937*. https://doi.org/10.1016/j.carres.2023.108937

Drug Bank Online. (2024). *Tyloxapol*. Retrieved from https://go.drugbank.com/drugs/DB06439. Accessed October 10, 2024.

Durrant Lab. (2024). *LogP*. Retrieved from https://durrantlab.pitt.edu/molmoda/docs/structures/molprop/logp/. Accessed October 10, 2024.

Dybiec, J., Baran, W., Dąbek, B., Fularski, P., Młynarska, E., Radzioch, E., Rysz, J., & Franczyk, B. (2023). Advances in treatment of dyslipidemia. *International Journal of Molecular Sciences, 24(17), Article 13288*. https://doi.org/10.3390/ijms241713288

El Hilaly, J., & Lyoussi, B. (2002). Hypoglycaemic effect of the lyophilised aqueous extract of *Ajuga iva* in normal and streptozotocin diabetic rats. *Journal of Ethnopharmacology, 80*(2–3), 109–113. https://doi.org/10.1016/s0378-8741(01)00407-x

Fan, X., Wu, H., Li, M., Hu, X., & Zhong, M. (2015). Isolation of polysaccharides from *Perna viridis* and their antioxidant activities in high-fat diet-fed mice. *Modern Food Science and Technology, 31*, 19–31. https://doi.org/10.13982/j.mfst.1673-9078.2015.12.004

Farmery, A. K., Alexander, K., Anderson, K., Blanchard, J. L., Carter, C. G., Evans, K., … Nowak, B. (2022). Food for all: Designing sustainable and secure future seafood systems. *Reviews in Fish Biology and Fisheries, 32*(1), 101–121. https://doi.org/10.1007/s11160-021-09663-x

de Freitas, C. M. P., Júnior, D. B. S., Martins, R. D., Dias, M. M. D. S., Coimbra, J. S. D. R., & de Sousa, R. C. S. (2021). Simulation of ethanol recovery and economic analysis of pectin production on an industrial scale. *Bioprocess and Biosystems Engineering, 44*(8), 1639–1647. https://doi.org/10.1007/s00449-021-02546-2

Gao, H., Wang, R., Wang, Y., Li, H., Lan, S., Zhao, M., … Li, W. (2024). Structural characterization and anti-inflammatory activity of novel acidic polysaccharides from Laoshan black tea. *Journal of Food Biochemistry, 2024 (1), Article 4709041*. https://doi.org/10.1155/2024/4709041

Gardner, J. P. A., Patterson, J., George, S., & Patterson, E. J. P. (2016). Combined evidence indicates that *Perna indica* Kuriakose and Nair 1976 is *Perna perna* (Linnaeus, 1758) from the Oman region introduced into southern India more than 100 years ago. *Biological Invasions, 18*(5), 1375–1390. https://doi.org/10.1007/s10530-016-1074-9

Gesto, D. S., Pereira, C. M. S., Cerqueira, N. M. F. S., & Sousa, S. F. (2020). An atomic-level perspective of HMG-CoA-reductase: The target enzyme to treat hypercholesterolemia. *Molecules, 25(17), Article 3891*. https://doi.org/10.3390/molecules25173891

Getachew, A. T., Lee, H. J., Cho, Y. J., Chae, S. J., & Chun, B. S. (2019). Optimization of polysaccharides extraction from Pacific oyster (*Crassostrea gigas*) using subcritical water: Structural characterization and biological activities. *International Journal of Biological Macromolecules, 121*, 852–861. https://doi.org/10.1016/j.ijbiomac.2018.10.091

Gobinath, R., Parasuraman, S., Sreeramanan, S., Enugutti, B., & Chinni, S. V. (2022). Antidiabetic and antihyperlipidemic effects of methanolic extract of leaves of *Spondias mombin* in streptozotocin-induced diabetic rats. *Frontiers in Physiology, 13, Article 870399*. https://doi.org/10.3389/fphys.2022.870399

Govindan, M. S., & Thomas, J. (2021). Anti-inflammatory activity of Sulphated polysaccharide isolated from *Ulva fasciata*. *International Journal for Research in Applied Science and Engineering Technology, 9*(11), 2041–2043. https://doi.org/10.22214/ijraset.2021.39176

Gu, J., Zhang, H., Wen, C., Zhang, J., He, Y., Ma, H., & Duan, Y. (2020). Purification, characterization, antioxidant and immunological activity of polysaccharide from *Sagittaria sagittifolia* L. *Food Research International, 136, Article 109345*. https://doi.org/10.1016/j.foodres.2020.109345

Guo, W. L., Deng, J. C., Pan, Y. Y., Xu, J. X., Hong, J. L., Shi, F. F., … Lv, X. C. (2020). Hypoglycemic and hypolipidemic activities of *Grifola frondosa* polysaccharides and their relationships with the modulation of intestinal microflora in diabetic mice induced by high-fat diet and streptozotocin. *International Journal of Biological Macromolecules, 153*, 1231–1240. https://doi.org/10.1016/j.ijbiomac.2019.10.253

Henriques, M. G., Silva, P. M., Martins, M. A., Flores, C. A., Cunha, F. Q., Assreuy-Filho, J., & Cordeiro, R. S. (1987). Mouse paw edema. A new model for inflammation?. *Brazilian journal of medical and biological research =. Revista brasileira de pesquisas medicas e biologicas, 20*(2), 243–249.

Hiebl, V., Schachner, D., Ladurner, A., Heiss, E. H., Stangl, H., & Dirsch, V. M. (2020). Caco-2 cells for measuring intestinal cholesterol transport: Possibilities and limitations. *Biological Procedures Online, 22, Article 7*. https://doi.org/10.1186/s12575-020-00120-w

Hong, T., Yin, J. Y., Nie, S. P., & Xie, M. Y. (2021). Applications of infrared spectroscopy in polysaccharide structural analysis: Progress, challenge and perspective. *Food Chemistry, X, 12, Article 100168*. https://doi.org/10.1016/j.fochx.2021.100168

Hou, C., Chen, L., Yang, L., & Ji, X. (2020). An insight into anti-inflammatory effects of natural polysaccharides. *International Journal of Biological Macromolecules, 153*, 248–255. https://doi.org/10.1016/j.ijbiomac.2020.02.315

Hsu, C. Y., Allela, O. Q. B., Hussein, A. M., Mustafa, M. A., Kaur, M., Alaraj, M., … Farhood, B. (2024). Recent advances in polysaccharide-based drug delivery systems for cancer therapy: a comprehensive review. *Artificial Cells, Nanomedicine, and Biotechnology, 52*(1), 564–586. https://doi.org/10.1080/21691401.2024.2436350

Huang, G., Chen, F., Yang, W., & Huang, H. (2021). Preparation, deproteinization, and comparison of bioactive polysaccharides. *Trends in Food Science & Technology, 109*, 564–568. https://doi.org/10.1016/j.tifs.2021.01.038

Huang, L., Shen, M., Morris, G. A., & Xie, J. (2019). Sulfated polysaccharides: Immunomodulation and signaling mechanisms. *Trends in Food Science & Technology, 92*, 1–11. https://doi.org/10.1016/j.tifs.2019.08.008

Huo, D. Y., Li, Y. F., Song, L. J., Zhang, W. X., Li, X. D., Zhang, J., … Li, W. (2025). Colon-targeted ginseng polysaccharides-based microspheres for improving ulcerative colitis via anti-inflammation and gut microbiota modulation. *Advanced Healthcare Materials, 14(6), Article 2404122*. https://doi.org/10.1002/adhm.202404122

Husain, S., Hillmann, K., Hengst, K., & Englert, H. (2023). Effects of a lifestyle intervention on the biomarkers of oxidative stress in non-communicable diseases: A systematic review. *Frontiers in Aging, 4, Article 1085511*. https://doi.org/10.3389/fragi.2023.1085511

Huynh, D. T. M., Huynh, T., Le, M. T., & Mai, H. N. (2024). Investigation of acute and sub-chronic oral toxicity and effects of *Allium ascalonicum* L. extract on Triton WR1339-induced hyperlipidemia on Swiss albino mice. *Pharmacological Research-Modern Chinese Medicine, 10, Article 100407*. https://doi.org/10.1016/j.prmcm.2024.100407

Jamioł-Milc, D., Biernawska, J., Liput, M., Stachowska, L., & Domiszewski, Z. (2021). *Seafood intake as a method of non-communicable diseases (NCD) prevention in adults. Nutrients, 13(5), Article 1422*. https://doi.org/10.3390/nu13051422

Jeyasanta, I., Sathish, N., & Patterson, J. (2020). Identification of bioactive peptides in mussel species of Kanyakumari coast. *Asian Journal of Biotechnology, 12*, 75–86. https://doi.org/10.3923/ajbkr.2020.75.86

Jeyasanta, I., Wilson, S., Sathish, N., & Patterson, J. (2018). Biochemical composition and heavy metal content in the mussels of Kadiyapattinam, Kanyakumari district, south west coast of India. *Journal of Nutritional Biology, 4*(2), 244–258. https://doi.org/10.18314/jnb.v4i2.1417

Ji, X., Peng, B., Ding, H., Cui, B., Nie, H., & Yan, Y. (2023). Purification, structure and biological activity of pumpkin polysaccharides: A review. *Food Reviews International, 39*(1), 307–319. https://doi.org/10.1080/87559129.2021.1904973

Jiang, N., Li, B., Wang, X., Xu, X., Liu, X., Li, W., Chang, X., Li, H., & Qi, H. (2020). The antioxidant and antihyperlipidemic activities of phosphorylated polysaccharide from *Ulva pertusa*. *International Journal of Biological Macromolecules, 145*, 1059–1065. https://doi.org/10.1016/j.ijbiomac.2019.09.198

Jing, Y. S., Ma, Y. F., Pan, F. B., Li, M. S., Zheng, Y. G., Wu, L. F., & Zhang, D. S. (2022). An insight into antihyperlipidemic effects of polysaccharides from natural resources. *, 27*(6),. *Molecules, 27(6), Article 1903*. https://doi.org/10.3390/molecules27061903

Kahnt, A. S., Angioni, C., Göbel, T., Hofmann, B., Roos, J., Steinbrink, S. D., … Maier, T. J. (2022). Inhibitors of human 5-lipoxygenase potently interfere with prostaglandin transport. *Frontiers in Pharmacology., 12, Article 782584*. https://doi.org/10.3389/fphar.2021.782584

Karthik, M. V., Satya Deepak, M. V., & Shukla, P. (2012). Explication of interactions between HMGCR isoform 2 and various statins through *in silico* modeling and docking. *Computers in Biology and Medicine, 42*(2), 156–163. https://doi.org/10.1016/j.compbiomed.2011.11.003

Kong, Y., Li, Y., Dai, Z. R., Qin, M., Fan, H. L., Hao, J. G., … Wang, P. (2021). Glycosaminoglycan from *Ostrea rivularis* attenuates hyperlipidemia and regulates gut microbiota in high-cholesterol diet-fed zebrafish. *Food Science and Nutrition, 9*(9), 5198–5210. https://doi.org/10.3390/molecules27061903

Lamantia, V., Sniderman, A., & Faraj, M. (2016). Nutritional management of hyperapoB. *Nutrition Research Reviews, 29*(2), 202–233. https://doi.org/10.3389/fphar.2021.782584

Lee, B. R., Kim, S. Y., Kim, D. W., An, J. J., Song, H. Y., Yoo, K. Y., … Eum, W. S. (2009). *Agrocybe chaxingu* polysaccharide prevents inflammation through the inhibition of COX-2 and NO production. *BMB Reports, 42*(12), 794–799. https://doi.org/10.5483/bmbrep.2009.42.12.794

Liu, F., Zhang, X., Li, Y., Chen, Q., Liu, F., Zhu, X., & Wang, F. (2017). Anti-inflammatory effects of a *Mytilus coruscus* α-D-glucan (MP-A) in activated macrophage cells via TLR4/NF-κB/MAPK pathway inhibition. *Marine Drugs, 15(9), Article 294*. https://doi.org/10.3390/md15090294

Liu, Y., Fang, S., Zhou, M., Shang, X., Yang, W., & Fu, X. (2018). Geographic variation in water-soluble polysaccharide content and antioxidant activities of *Cyclocarya paliurus* leaves. *Industrial Crops and Products, 121*, 180–186. https://doi.org/10.1016/j.indcrop.2018.05.017

Loram, L. C., Fuller, A., Fick, L. G., Cartmell, T., Poole, S., & Mitchell, D. (2007). Cytokine profiles during carrageenan-induced inflammatory hyperalgesia in rat muscle and hind paw. *The Journal of Pain, 8*(2), 127–136. https://doi.org/10.1016/j.jpain.2006.06.010

Lubbe, L., Cozier, G., Oosthuizen, D., Acharya, K., & Sturrock, E. (2020). ACE2 and ACE: Structure-based insights into mechanism, regulation and receptor recognition by SARS-CoV. *Clinical Science (London, England: 1979), 134*(21), 2851–2871. https://doi.org/10.1042/CS20200899

Mallya, P., & Lewis, S. A. (2024). Selecting an appropriate animal model for dyslipidemia. *Indian Journal of Pharmaceutical Education and Research, 58*(3s), s683–s692. https://doi.org/10.5530/ijper.58.3s.72

Martins, I. J. (2017). Autoimmune disease and mitochondrial dysfunction in chronic diseases. *Research on Chronic Diseases, 1*, 10–12.

Mashima, R., & Okuyama, T. (2015). The role of lipoxygenases in pathophysiology; new insights and future perspectives. *Redox Biology, 6*, 297–310. https://doi.org/10.1016/j.redox.2015.08.006

McNamara, C. R., Mandel-Brehm, J., Bautista, D. M., Siemens, J., Deranian, K. L., Zhao, M., … Fanger, C. M. (2007). TRPA1 mediates formalin-induced pain. *Proceedings of the National Academy of Sciences of the United States of America, 104*(33), 13525–13530. https://doi.org/10.1073/pnas.0705924104

Miao, M., Ma, Y., Jiang, B., Huang, C., Li, X., Cui, S. W., & Zhang, T. (2014). Structural investigation of a neutral extracellular glucan from *lactobacillus reuteri* SK24.003. *Carbohydrate Polymers, 106*, 384–392. https://doi.org/10.1016/j.carbpol.2014.01.047

Morris, C. J. (2003). *Carrageenan-induced paw edema in the rat and mouse. Methods in molecular biology (Clifton, N.J.), 225, 115–121*. https://doi.org/10.1385/1-59259-374-7:115

Murphy, C., Deplazes, E., Cranfield, C. G., & Garcia, A. (2020). The role of structure and biophysical properties in the pleiotropic effects of statins. *International Journal of Molecular Sciences, 21(22), Article 8745*. https://doi.org/10.3390/ijms21228745

Myers, M. J., Deaver, C. M., & Lewandowski, A. J. (2019). Molecular mechanism of action responsible for carrageenan-induced inflammatory response. *Molecular Immunology, 109*, 38–42. https://doi.org/10.1016/j.molimm.2019.02.020

Nair, A. B., & Jacob, S. (2016). A simple practice guide for dose conversion between animals and human. *Journal of Basic and Clinical Pharmacy, 7*(2), 27–31. https://doi.org/10.4103/0976-0105.177703

Nigam, M., Mishra, A. P., Deb, V. K., Dimri, D. B., Tiwari, V., Bungau, S. G., & Radu, A. F. (2023). Evaluation of the association of chronic inflammation and cancer: Insights and implications. *Biomedicine & Pharmacotherapy, 164, Article 115015*. https://doi.org/10.1016/j.biopha.2023.115015

Organization for Economic Co-operation and Development. (2002). *Test No. 420: Acute oral toxicity – Fixed dose-procedure. OECD Guidelines for the Testing of Chemicals, Volume 4, Number 420, OECD, Paris, France, OECD Publishing, 2002*. https://doi.org/10.1787/9789264070943-en

Ou, Z., Zhao, J., Zhu, L., Huang, L., Ma, Y., Ma, C., Luo, C., Zhu, Z., Yuan, Z., Wu, J., Li, R., & Yi, J. (2019). Anti-inflammatory effect and potential mechanism of betulinic acid on λ-carrageenan-induced paw edema in mice. *Biomedicine and Pharmacotherapy, 118, Article 109347*. https://doi.org/10.1016/j.biopha.2019.109347

Paget, G. E., & Barnes, J. M. (1964). *Toxicity test, in: D.R. Laurence, A.L. Bacharach (Eds.), Evaluation of drug activities: Pharmacometrics (pp. 135-366). Academic Press*.

Panzoldo, N. B., urban, A., Parra, E. S., Oliveira, R., Zago, V. S., da Silva, … de Faria, E. C. (2011). Differences and similarities of postprandial lipemia in rodents and humans. Lipids in health and disease, 10. *Article, 86*. https://doi.org/10.1186/1476-511X-10-86

Park, J. Y., Pillinger, M. H., & Abramson, S. B. (2006). Prostaglandin E2 synthesis and secretion: The role of PGE2 synthases. *Clinical immunology (Orlando, Fla.), 119*(3), 229–240. https://doi.org/10.1016/j.clim.2006.01.016

Paschou, S. A., Papadopoulou-Marketou, N., Chrousos, G. P., & Kanaka-Gantenbein, C. (2018). On type 1 diabetes mellitus pathogenesis. *Endocrine Connections, 7*(1), R38–R46. https://doi.org/10.1530/EC-17-0347

Patil, K. R., Mahajan, U. B., Unger, B. S., Goyal, S. N., Belemkar, S., Surana, S. J., & Patil, C. R. (2019). Animal models of inflammation for screening of anti-inflammatory drugs: Implications for the discovery and development of phytopharmaceuticals. *International Journal of Molecular Sciences, 20(18), Article 4367*. https://doi.org/10.3390/ijms20184367

Pedrosa, L. F., de Vos, P., & Fabi, J. P. (2023). Nature's soothing solution: Harnessing the potential of food-derived polysaccharides to control inflammation. *Current research. Structural Biology, 6, Article 100112*. https://doi.org/10.1016/j.crstbi.2023.100112

Ram, B. S., Venu, S., Swapna, B. M. A., Kumar, R. R., & Narayan, S. (2016). Studies on biometrics and proximate composition of *Perna indica*, Kuriakose & Nair, 1976, collected from Sippighat, south Andaman. *Life Sciences Leaflets, 82*, 1–12. https://doi.org/10.7860/JCDR/2016/18890.7993

Ramamoorthy, S., & Cidlowski, J. A. (2016). Corticosteroids: Mechanisms of action in health and disease. *Rheumatic diseases clinics of North America, 42*(1), 15–31. https://doi.org/10.1016/j.rdc.2015.08.002

Rasouli, M., Tahmouri, H., & Mosavi-Mehr, M. (2016). The long-term kinetic of plasma lipids and lipoproteins in tyloxapol-injected rats. *Journal of Clinical and Diagnostic Research: JCDR, 10*(6), BF01–BF5. https://doi.org/10.7860/JCDR/2016/18890.7993

Rjeibi, I., Feriani, A., Hentati, F., Hfaiedh, N., Michaud, P., & Pierre, G. (2019). Structural characterization of water-soluble polysaccharides from *Nitraria retusa* fruits and their antioxidant and hypolipidemic activities. *International Journal of Biological Macromolecules, 129*, 422–432. https://doi.org/10.1016/j.ijbiomac.2019.02.049

Seyedsadjadi, N., & Grant, R. (2020). *The potential benefit of monitoring oxidative stress and inflammation in the prevention of non-communicable diseases (NCDs). Antioxidants (Basel, Switzerland), 10(1), Article 15*. https://doi.org/10.3390/antiox10010015

Sharma, J. N., Al-Omran, A., & Parvathy, S. S. (2007). Role of nitric oxide in inflammatory diseases. *Inflammopharmacology, 15*(6), 252–259. https://doi.org/10.1007/s10787-007-0013-x

Shehzad, A., Ha, T., Subhan, F., & Lee, Y. S. (2011). New mechanisms and the anti-inflammatory role of curcumin in obesity and obesity-related metabolic diseases. *European Journal of Nutrition, 50*(3), 151–161. https://doi.org/10.1007/s00394-011-0188-1

Shen, X., Wei, H., Li, J., Wei, W., Zhang, B., Lu, C., & Li, Y. (2022). Ectopic colonization and immune landscapes of periodontitis microbiota in germ-free mice with streptozotocin-induced type 1 diabetes mellitus. *Frontiers in Microbiology, 13, Article 889415*. https://doi.org/10.3389/fmicb.2022.889415

Silva Dos Santos, F., Neves, R. A. F., Crapez, M. A. C., Teixeira, V. L., & Krepsky, N. (2022). How does the brown mussel *Perna perna* respond to environmental pollution? A review on pollution biomarkers. *Journal of Environmental Sciences, 111*, 412–428. https://doi.org/10.1016/j.jes.2021.04.006

Suchecka, D., Gromadzka-Ostrowska, J., Żyła, E., Harasym, J., & Oczkowski, M. (2017). Selected physiological activities and health-promoting properties of cereal beta-glucans: A review. *Journal of Animal and Feed Sciences, 26*, 181–191. https://doi.org/10.22358/jafs/70066/2017

Taddei, S., & Bortolotto, L. (2016). Unraveling the pivotal role of bradykinin in ACE inhibitor activity. *American Journal of Cardiovascular Drugs: Drugs, Devices, and Other Interventions, 16*(5), 309–321. https://doi.org/10.1007/s40256-016-0173-4

Tan, K., Lu, S. Y., Tan, K., Ransangan, J., Cai, X., & Cheong, K. L. (2023). Bioactivity of polysaccharides derived from bivalves. *International Journal of Biological Macromolecules, 250, Article 126096*. https://doi.org/10.1016/j.ijbiomac.2023.126096

Tatarkiewicz, J., Rzodkiewicz, P., Żochowska, M., Staniszewska, A., & Bujalska-Zadrożny, M. (2019). New antihistamines - perspectives in the treatment of some allergic and inflammatory disorders. *Archives of Medical Science : AMS, 15*(2), 537–553. https://doi.org/10.5114/aoms.2017.68534

Tirado, L. C. E., & Yassin, L. M. (2017). B cells interactions in lipid immune responses: Implications in atherosclerotic disease. *Lipids in Health and Disease, 16(1), Article 30*. https://doi.org/10.1186/s12944-016-0390-5

Udomkasemsab, A., & Prangthip, P. (2019). High fat diet for induced dyslipidemia and cardiac pathological alterations in Wistar rats compared to Sprague Dawley rats. *Clínica e Investigación en Arteriosclerosis, 31*(2), 56–62. https://doi.org/10.1016/j.arteri.2018.09.004

Utami, D., Wahyudi, R., & Widyaningsih, W. (2023). The sulphated polysaccharide compounds from green algae (*Ulva lactuca* L) as a potential natural anti-inflammatory agent based on molecular docking study targeting cyclooxygenase-2 receptor. *Pharmaciana, 13*(2), 146–158. https://doi.org/10.12928/pharmaciana.v13i2.25848

Vaure, C., & Liu, Y. (2014). A comparative review of toll-like receptor 4 expression and functionality in different animal species. *Frontiers in Immunology, 5, Article 316*. https://doi.org/10.3389/fimmu.2014.00316

Wan, X. Z., Ai, C., Chen, Y. H., Gao, X. X., Zhong, R. T., Zhong, R. T., … Zhao, C. (2019). Physicochemical characterization of a polysaccharide from green microalga *Chlorella pyrenoidosa* and its hypolipidemic activity via gut microbiota regulation in rats. *Journal of Agricultural and Food Chemistry, 68*(5), 1186–1197. https://doi.org/10.1021/acs.jafc.9b06282

Wang, B., Yan, L., Guo, S., Wen, L., Yu, M., Feng, L., & Jia, X. (2022). Structural elucidation, modification, and structure-activity relationship of polysaccharides in Chinese herbs: A review. *Frontiers. Nutrition, 9, Article 908175*. https://doi.org/10.3389/fnut.2022.908175

Wang, R., Yang, X., Jiang, Q., Chen, L., Gu, S., Shen, G., & ...Xiang, X. (2023). Effect of mussel polysaccharide on glucolipid metabolism and intestinal flora in type 2 diabetic mice. *Journal of the Science of Food and Agriculture, 103*(7), 3353–3366. https://doi.org/10.1002/jsfa.12488

Wang, Y. Y., Zhu, J., Ma, H., Ding, Z. C., Li, L., & Yan, J. K. (2019). Antidiabetic activity of a polysaccharide-protein complex from Asian clam (*Corbicula fluminea*) in streptozotoxin-induced diabetic rats and its underlying mechanism. *Food & Function, 10*(9), 5574–5586. https://doi.org/10.1039/c9fo01341e

Wang, Z., Wang, Z., Huang, W., Suo, J., Chen, X., Ding, K., & ...Zhang, H. (2020). Antioxidant and anti-inflammatory activities of an anti-diabetic polysaccharide extracted from *Gynostemma pentaphyllum* herb. *International Journal of Biological Macromolecules, 145*, 484–491. https://doi.org/10.1016/j.ijbiomac.2019.12.213

Wold, C. W., Christopoulos, P. F., Arias, M. A., Dzovor, D. E., Øynebråten, I., Corthay, A., & Inngjerdingen, K. T. (2024). Fungal polysaccharides from *Inonotus obliquus* are agonists for toll-like receptors and induce macrophage anti-cancer activity. *Communications Biology, 7(1), Article 222*. https://doi.org/10.1038/s42003-024-05853-y

Wu, J., Shao, H., Zhang, J., Ying, Y., Cheng, Y., Zhao, D., & ...Ling, P. (2019). Mussel polysaccharide α-D-glucan (MP-A) protects against non-alcoholic fatty liver disease via maintaining the homeostasis of gut microbiota and regulating related gut-liver axis signaling pathways. *International Journal of Biological Macromolecules, 130*, 68–78. https://doi.org/10.1016/j.ijbiomac.2019.02.097

Wu, Q., Wang, Q., Fu, J., & Ren, R. (2019). Polysaccharides derived from natural sources regulate triglyceride and cholesterol metabolism: A review of the mechanisms. *Food & Function, 10*(5), 2330–2339. https://doi.org/10.1039/c8fo02375a

Wu, Y., Jiang, H., Lin, J. S., Liu, J., Wu, C. J., & Xu, R. (2020). Antioxidant, hypolipidemic and hepatic protective activities of polysaccharides from

Phascolosoma esculenta. *Marine Drugs, 18(3), Article 158*. https://doi.org/10.3390/md18030158

Xiang, X., Jiang, Q., Yang, H., Zhou, X., Chen, Y., Chen, H., … Chen, L. (2022). A review on shellfish polysaccharides: Extraction, characterization and amelioration of metabolic syndrome. *Frontiers in Nutrition., 9*. Article 974860 doi:10.3389/fnut.2022.974860.

Xiang, X. W., Wang, R., Yao, L. W., Zhou, Y. F., Sun, P. L., Zheng, B., & Chen, Y. F. (2021). Anti-inflammatory effects of *Mytilus coruscus* polysaccharide on RAW264.7 cells and DSS-induced colitis in mice. *Marine Drugs, 19(8), Article 468*. https://doi.org/10.3390/md19080468

Xue, H., Hao, Z., Gao, Y., Cai, X., Tang, J., Liao, X., & Tan, J. (2023). Research progress on the hypoglycemic activity and mechanisms of natural polysaccharides. *International Journal of Biological Macromolecules, 252, Article 126199*. https://doi.org/10.1016/j.ijbiomac.2023.126199

Zarghi, A., & Arfaei, S. (2011). Selective COX-2 inhibitors: A review of their structure-activity relationships. *Iranian Journal of Pharmaceutical Research : IJPR, 10*(4), 655–683.

Zhan, H., Song, T., Yu, G., Jiang, Z., Du, X., Zhu, Y., … Li, Q. (2021). Hypolipidemic activity of polysaccharides purified from *Bangia fuscopurpurea*. *Food Science, 42*(7), 142–148. https://doi.org/10.7506/spkx1002-6630-20200302-024

Zhang, Y., Ren, C., Lu, G., Mu, Z., Cui, W., Gao, H., & Wang, Y. (2014). Anti-diabetic effect of mulberry leaf polysaccharide by inhibiting pancreatic islet cell apoptosis and ameliorating insulin secretory capacity in diabetic rats. *International Immunopharmacology, 22*(1), 248–257. https://doi.org/10.1016/j.intimp.2014.06.039

Zhang, Z., Zeng, Z., Wang, L., Xiong, B., Zheng, B., Zhang, Y., & Pan, L. (2025). *Dictyophora indusiata* polysaccharide attenuated LPS-induced intestinal inflammation of mice via the TLR4/JNK signaling pathway. *Journal of the Science of Food and Agriculture, 105*(2), 974–981. https://doi.org/10.1002/jsfa.13888

Zhu, B. T. (2022). Pathogenic mechanism of autoimmune diabetes mellitus in humans: Potential role of streptozotocin-induced selective autoimmunity against human islet *β*-cells. *Cells, 11 (3), Article 492*. https://doi.org/10.3390/cells11030492

Zhukova, N. V., Novgorodtseva, T. P., & Denisenko, Y. K. (2014). Effect of the prolonged high-fat diet on the fatty acid metabolism in rat blood and liver. *Lipids in Health and Disease, 13, Article 49*. https://doi.org/10.1186/1476-511X-13-49

Zhang, Y., Lu, J., Li, H., & Song, H. (2025). Advances in dietary polysaccharides as hypoglycemic agents: Mechanisms, structural characteristics, and innovative applications. *Critical Reviews in Food Science and Nutrition, 65*(8), 1383–1403. https://doi.org/10.1080/10408398.2023.2293254